International Journal of Physical Sciences

Volume 10 Number 17 16 September 2015

ISSN 1992-1950

Academic Journals

ABOUT IJPS

The **International Journal of Physical Sciences (IJPS)** is published weekly (one volume per year) by Academic Journals.

International Journal of Physical Sciences (IJPS) is an open access journal that publishes high-quality solicited and unsolicited articles, in English, in all Physics and chemistry including artificial intelligence, neural processing, nuclear and particle physics, geophysics, physics in medicine and biology, plasma physics, semiconductor science and technology, wireless and optical communications, materials science, energy and fuels, environmental science and technology, combinatorial chemistry, natural products, molecular therapeutics, geochemistry, cement and concrete research, metallurgy, crystallography and computer-aided materials design. All articles published in IJPS are peer-reviewed.

Contact Us

Editorial Office: ijps@academicjournals.org

Help Desk: helpdesk@academicjournals.org

Website: http://www.academicjournals.org/journal/IJPS

Submit manuscript online http://ms.academicjournals.me/

Editors

Prof. Sanjay Misra
Department of Computer Engineering, School of Information and Communication Technology
Federal University of Technology, Minna,
Nigeria.

Prof. Songjun Li
School of Materials Science and Engineering,
Jiangsu University,
Zhenjiang,
China

Dr. G. Suresh Kumar
Senior Scientist and Head Biophysical Chemistry
Division Indian Institute of Chemical Biology
(IICB)(CSIR, Govt. of India),
Kolkata 700 032,
INDIA.

Dr. 'Remi Adewumi Oluyinka
Senior Lecturer,
School of Computer Science
Westville Campus
University of KwaZulu-Natal
Private Bag X54001
Durban 4000
South Africa.

Prof. Hyo Choi
Graduate School
Gangneung-Wonju National University
Gangneung,
Gangwondo 210-702, Korea

Prof. Kui Yu Zhang
Laboratoire de Microscopies et d'Etude de Nanostructures (LMEN)
Département de Physique, Université de Reims,
B.P. 1039. 51687,
Reims cedex,
France.

Prof. R. Vittal
Research Professor,
Department of Chemistry and Molecular Engineering
Korea University, Seoul 136-701,
Korea.

Prof Mohamed Bououdina
Director of the Nanotechnology Centre
University of Bahrain
PO Box 32038,
Kingdom of Bahrain

Prof. Geoffrey Mitchell
School of Mathematics,
Meteorology and Physics
Centre for Advanced Microscopy
University of Reading Whiteknights,
Reading RG6 6AF
United Kingdom.

Prof. Xiao-Li Yang
School of Civil Engineering,
Central South University,
Hunan 410075,
China

Dr. Sushil Kumar
Geophysics Group,
Wadia Institute of Himalayan Geology,
P.B. No. 74 Dehra Dun - 248001(UC)
India.

Prof. Suleyman KORKUT
Duzce University
Faculty of Forestry
Department of Forest Industrial Engineeering
Beciyorukler Campus 81620
Duzce-Turkey

Prof. Nazmul Islam
Department of Basic Sciences & Humanities/Chemistry,
Techno Global-Balurghat, Mangalpur, Near District Jail P.O: Beltalapark, P.S: Balurghat, Dist.: South Dinajpur,
Pin: 733103,India.

Prof. Dr. Ismail Musirin
Centre for Electrical Power Engineering Studies (CEPES), Faculty of Electrical Engineering, Universiti Teknologi Mara,
40450 Shah Alam,
Selangor, Malaysia

Prof. Mohamed A. Amr
Nuclear Physic Department, Atomic Energy Authority
Cairo 13759,
Egypt.

Dr. Armin Shams
Artificial Intelligence Group,
Computer Science Department,
The University of Manchester.

Editorial Board

Prof. Salah M. El-Sayed
Mathematics. Department of Scientific Computing.
Faculty of Computers and Informatics,
Benha University. Benha ,
Egypt.

Dr. Rowdra Ghatak
Associate Professor
Electronics and Communication Engineering Dept.,
National Institute of Technology Durgapur
Durgapur West Bengal

Prof. Fong-Gong Wu
College of Planning and Design, National Cheng Kung University
Taiwan

Dr. Abha Mishra.
Senior Research Specialist & Affiliated Faculty.
Thailand

Dr. Madad Khan
Head
Department of Mathematics
COMSATS University of Science and Technology
Abbottabad, Pakistan

Prof. Yuan-Shyi Peter Chiu
Department of Industrial Engineering & Management
Chaoyang University of Technology
Taichung, Taiwan

Dr. M. R. Pahlavani,
Head, Department of Nuclear physics,
Mazandaran University,
Babolsar-Iran

Dr. Subir Das,
Department of Applied Mathematics,
Institute of Technology, Banaras Hindu University,
Varanasi

Dr. Anna Oleksy
Department of Chemistry
University of Gothenburg
Gothenburg,
Sweden

Prof. Gin-Rong Liu,
Center for Space and Remote Sensing Research
National Central University, Chung-Li,
Taiwan 32001

Prof. Mohammed H. T. Qari
Department of Structural geology and remote sensing
Faculty of Earth Sciences
King Abdulaziz UniversityJeddah,
Saudi Arabia

Dr. Jyhwen Wang,
Department of Engineering Technology and Industrial Distribution
Department of Mechanical Engineering
Texas A&M University
College Station,

Prof. N. V. Sastry
Department of Chemistry
Sardar Patel University
Vallabh Vidyanagar
Gujarat, India

Dr. Edilson Ferneda
Graduate Program on Knowledge Management and IT,
Catholic University of Brasilia,
Brazil

Dr. F. H. Chang
Department of Leisure, Recreation and Tourism Management,
Tzu Hui Institute of Technology, Pingtung 926,
Taiwan (R.O.C.)

Prof. Annapurna P.Patil,
Department of Computer Science and Engineering,
M.S. Ramaiah Institute of Technology, Bangalore-54,
India.

Dr. Ricardo Martinho
Department of Informatics Engineering, School of Technology and Management, Polytechnic Institute of Leiria, Rua General Norton de Matos, Apartado 4133, 2411-901 Leiria,
Portugal.

Dr Driss Miloud
University of mascara / Algeria
Laboratory of Sciences and Technology of Water
Faculty of Sciences and the Technology
Department of Science and Technology
Algeria

Prof. Bidyut Saha,
Chemistry Department, Burdwan University, WB,
India

International Journal of Physical Sciences

Table of Contents: Volume 10 Number 17, 16 September, 2015

ARTICLES

academicJournals

Vol. 10(17), pp. 503-519, 16 September, 2015
DOI: 10.5897/IJPS2015.4392
Article Number: 2845BB055494
ISSN 1992 - 1950
Copyright ©2015
Author(s) retain the copyright of this article
http://www.academicjournals.org/IJPS

International Journal of Physical Sciences

Full Length Research Paper

A case study of aeromagnetic data interpretation of Nsukka area, Enugu State, Nigeria, for hydrocarbon exploration

Daniel N. Obiora[1]*, Mirianrita N. Ossai[1] and Emmanuel Okwoli[2]

[1]Department of Physics and Astronomy, University of Nigeria, Nsukka, Enugu State, Nigeria.
[2]Department of Physics, Kogi state University, Anyigba, Kogi State, Nigeria.

Received 22 July, 2015; Accepted 19 August, 2015

The aeromagnetic data of Nsukka area was interpreted qualitatively and quantitatively. Standard Euler deconvolution, Source Parameter Imaging (SPI), Forward and Inverse modeling techniques were employed in quantitative interpretation with the aim of determining depth/thickness of the sedimentary Basin, magnetic susceptibilities and type of mineralization prevalent in the area. Oasis montaj 6.4.2 software and potent Q 4.10.07 software were employed in the data analysis. Forward and inverse modeling estimated depths for profiles 1, 2, 3, 4 and 5 were 1644, 2285, 1972, 2193 and 1200 m respectively, with respective susceptibility values of 0.0031, 0.0073, 1.4493, 0.0069 and 0.0016 which indicate dominance of iron rich minerals like limonite, hematite, pyrrhotite and pyrite, and forms lateritic caps on sandstones. Results from SPI estimated depth ranges from 151.6 m (outcropping and shallow magnetic bodies) to 3082.7 m (deep lying magnetic bodies). Depths of shallow magnetic sources resulting from lateritic bodies in the outcrops within the study area as estimated by Euler depths for the four different structural index (SI = 0.5, 1, 2, 3) ranges from 7.99 to 128.93 m. 35 to 150 m depth are good potential water reservoirs for Nsukka and environs. Depths of 1644 to 3082.7 m show sufficiently thick sediments suitable for hydrocarbon accumulation.

Key words: Aeromagnetic data, Nsukka area, Source Parameter Imaging (SPI), Euler deconvolution, forward and inverse modeling, anomalous source.

INTRODUCTION

The search for mineral deposits and hydrocarbon has been a major business challenge in Nigeria since the pre-colonial era and the 1960's respectively. The bedrock of Nigeria's economy before the discovery of oil had been the solid minerals and agricultural sectors, but currently, it is the oil and gas sector. Over 80% of the country's revenue comes from export and domestic sales of oil and gas. As the hydrocarbon potentials of the prolific Niger Delta becomes depleted or in the near future may be exhausted due to continuous exploitation, attention needs to be shifted to other sedimentary Basins. The lower Benue Trough, Nsukka in particular, is one of those

*Corresponding author. E-mail: daniel.obiora@unn.edu.ng
Author(s) agree that this article remain permanently open access under the terms of the Creative Commons Attribution License 4.0 International License

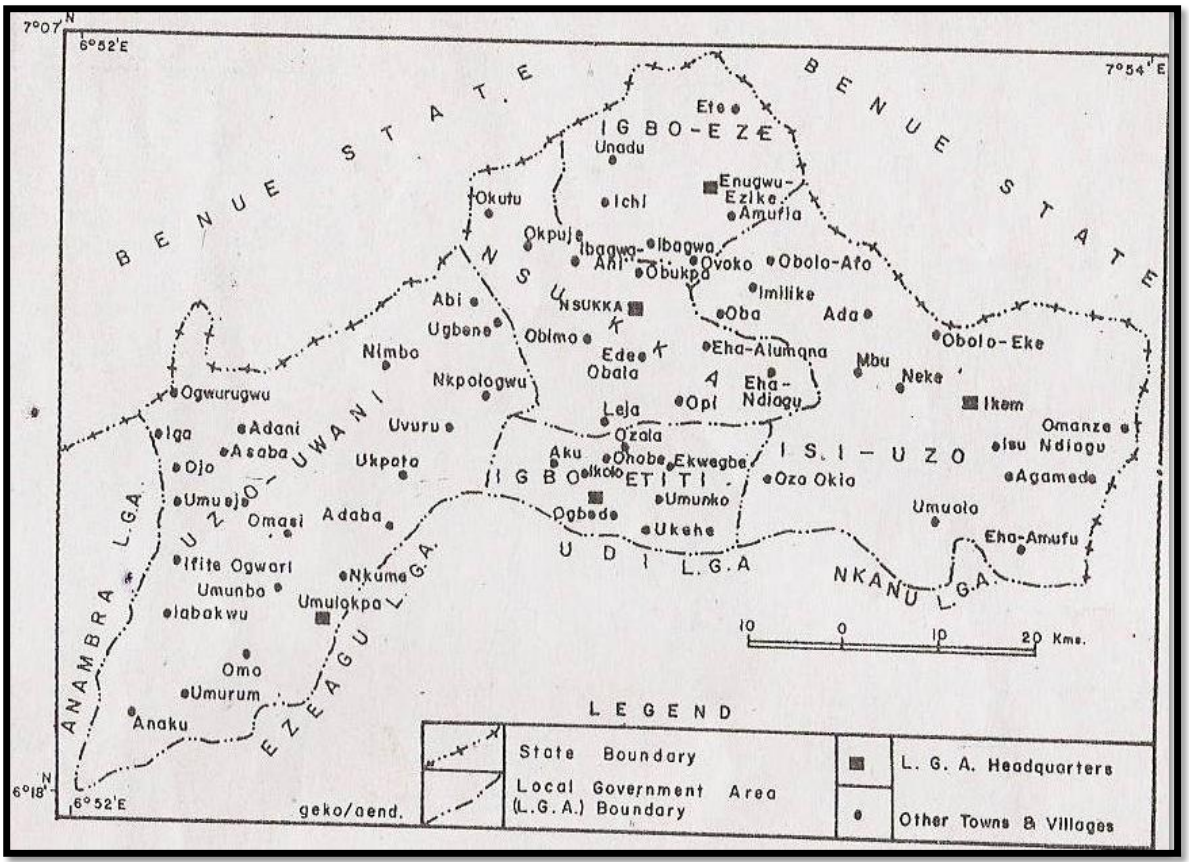

Figure 1. Map showing Nsukka area (Nwachukwu, 1972).

Basins being suspected to have high hydrocarbon potential, besides other economic mineral deposits concentration. The Benue Trough of Nigeria is a major tectonic feature in West Africa. It is an elongated rifted depression that trends NE-SW from the south, where it merges with the Niger Delta, to the north, where its sediments are part of the Chad Basin successions. The Benue Trough attains an approximate length of 800 km. It has a width of 130 to 150 km and is filled with Cretaceous sediments whose ages range from Middle Albian to Maestrichtian. Their thickness varies from about 6 km in the Lower Benue to about 5 km in the Upper Benue. The origin and evolution of the Benue Trough of Nigeria is fairly documented (Wright, 1976; Petters, 1978; Ofoegbu, 1985). Generally, the Benue Trough is believed to have been formed when the South America separated from Africa (Petters, 1978). The major component units of the Lower Benue Trough include the Anambra Basin, the Abakaliki Anticlinorium and the Afikpo Syncline.

The Nsukka area is a sedimentary Basin within the Anambra Basin which is part of the lower Benue Trough. There was a speculation in 2007 that a part of Nsukka area (Towns within Uzo-Uwani, Opi Agu and Eha-Ndiagu, Figure 1) has a good quantity of oil. An Oil company visited the area and carried out a preliminary survey work. Though their report is not yet made known to the public, but some geoscientists believe that the area contains more gas than oil.

There are some published works in the lower Benue Trough based on aeromagnetic data interpretations which employed different methods (Ofoegbu, 1984; Okeke, 1992; Onwuemesi, 1997; Ugbor and Okeke, 2010; Onu et al., 2011; Onuba et al., 2011; Ugwu and Ezema, 2012; Adetona and Abu, 2013; Igwesi and Umego, 2013; Ugwu et al., 2013; Ezema et al., 2014). The publications are based on the depths to basements/magnetic source bodies over the Lower Benue Trough and Anambra Basin in which Nsukka and environs falls, though no specific work had been carried out on Nsukka area. Ofoegbu (1984) interpreted the aeromagnetic anomalies over the Lower and Middle Benue Trough in terms of basic intrusive bodies which may occur either within the Cretaceous rocks or within the basement or both. He obtained a depth ranging from 0.5 to 7 km in the lower and middle Benue Basin and concluded that, although some of the observed anomalies could be attributed to the basement underneath the Benue Trough, the magnetic anomalies could not be satisfactorily interpreted fully in terms of a basement of variable topography. Such an interpretation

leads to a basement of too high a magnetization, basement outcrops and too thick a sedimentary cover in places not in agreement with the known geology of the area. The results of his study suggested that the magnetic anomalies over the Lower and Middle Trough are in the main caused by sizeable intrusive bodies of basic composition which can either lie within the sedimentary rocks or within the basement or both. The magnetic anomalies over the Lower and Middle Benue Trough are therefore due to the combined effect of a basement of variable thickness and topography and basic intrusive bodies.

Onwuemesi (1997) evaluated the depth to the basement (sedimentary thickness) in the Anambra Basin which is part of the lower Benue Trough to vary from 0.9 to 5.6 km. In the work of Igwesi and Umego (2013), they interpreted the aeromagnetic anomalies over some part of lower Benue Trough, using Spectral analysis which indicated a two layer source model with depth for deeper magnetic source ranging from 1.16 to 6.13 km with average of 3.03 km and depth to the shallower magnetic source ranging from 0.016 to 0.37 km with average of 0.22 km. Onu et al. (2011) estimated that the depths to the magnetic source bodies in the lower Benue Trough and some adjoining areas vary from 0.518 to 8.65 km with a mean depth of 3.513 km (for deeper magnetic source bodies) and 0.235 to 3.91 km with a mean depth of 1.389 km (for shallower magnetic source bodies). Onuba et al. (2011) interpreted the aeromagnetic anomalies over Okigwe area (Okigwe is within the Lower Benue Trough) and estimated the depth to basement using slope methods. They established two depth models varying from 2.18 to 4.91 km for deeper sources while the shallower sources vary from 0.55 to 1.82 km. However, they did not recommend hydrocarbon exploration in the area since the area has low thickness of sediments on the average. Adetona and Abu (2013) estimated the thickness of sedimentation within the Lower Benue Basin and Upper Anambra Basin. They employed spectral depth analysis which used the radial average energy spectrum to obtain a depth of 7.3 km and source parameter imaging to obtain a depth of 9.847 km. Also, Ezema et al. (2014) used forward and inverse modeling (potent software) to interpret the aeromagnetic data of Abakaliki which showed maximum depths of 4.96 to 9.8 km with minimum depths ranging from 0.12 to 0.17 km. These studies were carried out within the Lower Benue Trough in which Nsukka area falls, but none of the studies was carried out specifically in Nsukka area. This prompted our carrying out this work in Nsukka area, hence the first of its kind in that area.

The purpose of this study is to interpret qualitatively and quantitatively the aeromagnetic data of Nsukka area in southeastern Nigeria, using the standard Euler deconvolution, source parameter imaging (SPI) and forward and inverse modeling methods. These will include the determination of: (i) the susceptibilities of rock types in the area, (ii) the depth of the anomalous bodies, (iii) the dip, plunge and type of body causing the magnetic anomaly, and (iv) possible mineralization in the area. The results of this study will be compared with the results of previous works carried out in the lower Benue Trough and it will throw more light to the knowledge of subsurface structure in Nsukka area.

Geology and stratigraphy of the study area

The Nsukka sheet (covering the aeromagnetic data of Nsukka area) lies between latitudes 6°30′ and 7°00′ North and longitudes 7°00′ and 7°30′ East. It covers a total surface area of approximately 3,961 km^2. Nsukka is a sedimentary Basin within the Anambra Basin underlain by rocks which range in age from Coniacian to Paleocene. Anambra Basin consist of six major rock formations namely Enugu shale, Agwu shale, Mamu formation, Ajali formation, Nsukka formation and Imo shale formation. These rocks are grouped into four formations namely: Mamu formation, Ajali Sandstone, Nsukka Formation, and Imo Shale Formation (Nwajide and Reijers, 1995; Onwuemesi, 1995). Sediments deposited within this time interval occur in four distinct physiographic provinces, namely the Cross River plains, the Escarpment, the Plateau and the Anambra Plains. It was discovered that over 3,965 m of sediments comprising shales, sandstones, limestone and coal, were deposited in the area. Their environment of deposition varied from marine, through brackish water to entirely continental. Some of these sediments are of considerable economic importance and contain reserves of coal, natural gas, glass sands and considerable prospects for liquid hydrocarbon. The soil is rich and sustains a virile rural agriculture. The highest point in the area is about 590 m above datum plane but the lowlands generally have heights below 250 m above sea level. There are several elongated and conical hills separated by dry and wet valleys.

The geology of Nsukka area and environs is composed mainly of Imo Formation of Paleocene, Nsukka Formation, Ajali Formation of Maastichtian, Mamu Formation (Nwajide and Reijers, 1995; Onwuemesi, 1995). Figure 2 shows the geologic map of Nsukka Area.

Source of data

Data covering the Nsukka sheet was acquired from the Nigerian Geological Survey Agency. This survey was conducted in three phases between 2005 and 2010 as part of a major project known as the Sustainable Management for Mineral Resources by FURGO Airborne surveys. The survey has a Tie-line spacing of 500 m, the flight line along East-West direction with 100 m spacing, altitude of 80 m and terrain clearance of 100 m. Nsukka

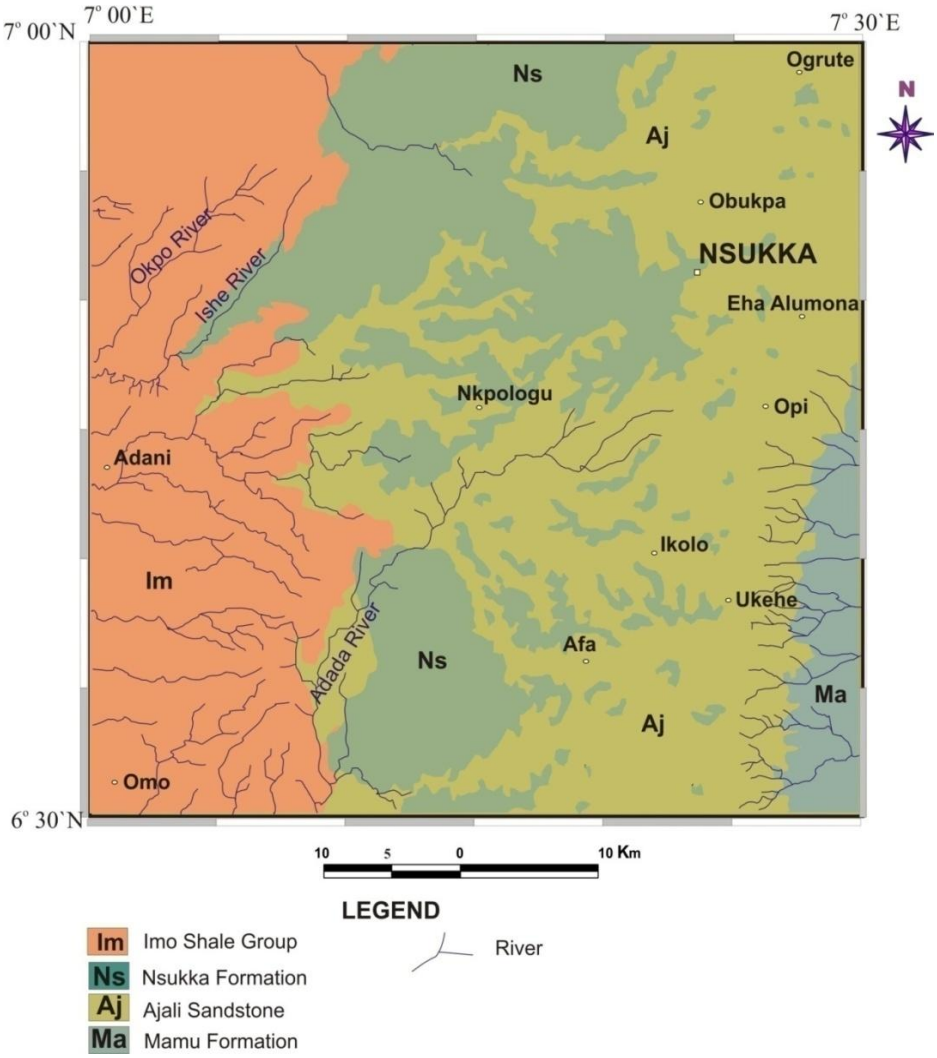

Figure 2. Geological map of the study area.

data was recorded in digitized form (X, Y, Z text file) after removing the geomagnetic gradient from the raw data using International Geomagnetic Reference Field (IGRF), 2010, with intensity of 33095 nT (nanoTesla), angles of inclination and declination of -13.988° and -1.902°, respectively. The X and Y represent the longitude and latitude of Nsukka in meters respectively, while the Z represents the magnetic field intensity measured in nanoTesla.

METHODS AND DATA ANALYSIS

Qualitative as well as quantitative interpretations were employed in this work. Qualitative interpretation of the field data was first carried out by inspecting the total magnetic intensity (TMI) grid of the study area. The total magnetic intensity map of the area was produced into maps which are in colour aggregate. Source Parameter Imaging (SPI), standard Euler deconvolution and Forward and Inverse modeling methods were employed in quantitative interpretation.

The initial stages of quantitative magnetic data interpretation involved the application of mathematical filters (reduction to pole, upward-downward continuation, first vertical derivative and horizontal derivative) to observed data. The specific goals of these filters vary, depending on the situation. The general purpose is to enhance anomalies of interest and to gain some basic information on source location or magnetization. The upward projection (upward continuation) operation smoothen the anomalies obtained at the ground surface by projecting the surface mathematically upward above the original datum (Revees, 2005). By implementation of reduction to pole on both the amplitude and phase spectra of the original TMI grid, the shapes of the magnetic anomalies were simplified so that they appeared like the positive anomalies located directly above the source expected for induce magnetized bodies at the magnetic pole where the angle of inclination is 90° and zero declination.

A derivative helped to sharpen the edges of anomaly and enhanced shallow features (Revees, 2005). This includes first and second vertical derivatives, and horizontal derivative. Computation of the first vertical derivative in an aeromagnetic survey is equivalent to observing the vertical gradient with a magnetic gradiometer with advantages of sharpening the edges of magnetic

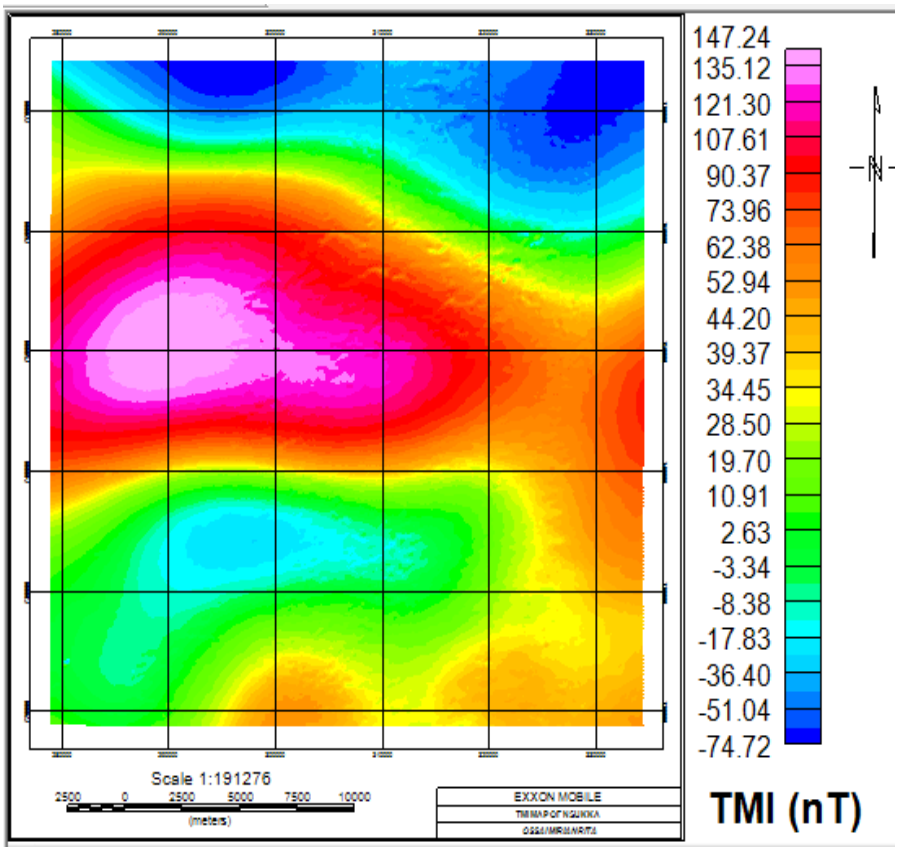

Figure 3. Total magnetic intensity (TMI) map of the study area.

anomalies, enhancing shallow magnetic sources, suppressing deeper magnetic sources and giving a better resolution of closely-spaced sources. Horizontal derivative was also calculated in the x and y directions.

Source parameter imaging, standard Euler deconvolution, forward and inverse modeling were used to evaluate the depths of magnetic source bodies. Source parameter imaging (SPI) method calculated source parameters for gridded magnetic data. The method assumes either a 2D slopping contact or a 2D dipping thin-sheet model and is based on the complex analytic signal. The SPI depth of magnetic data was determined using Oasis Montaj software and employing the first vertical derivatives and horizontal gradient. SPI method made the task of interpreting magnetic data significantly easier. This model was displayed on an image and the correct depth estimate for each anomaly determined.

The Euler deconvolution utilizes Euler's homogeneity relation proposed by Thompson (1982) and (Reid et al., 1990). It is a valuable tool for locating the position and depth of anomalous sources. OASIS MONTAJ software was employed in computing the Euler-3D image and depth.

Potent Q 4.10.07 software was used for the modeling and inversion of the anomalies after getting preliminary information about anomaly causative sources. Potent is a program for modeling the magnetic and gravitational effects of subsurface. It provides a highly interactive 3-D environment that, among other applications, is well suited for detailed ore body modeling for mineral exploration. The main concepts in potent Q 4.10.07 include: Observation, inversion, model, visualization and calculation. Interpretation of magnetic field data using potent software started with observation of the image of the observed data. The first step in interpreting the observed data was to take profiles on the field image. In interpreting the observed data, five profiles were taken along different parts of the field image.

RESULTS

The total magnetic intensity map of Nsukka area was produced into map (Figure 3) from the qualitative interpretation, which is in different colour aggregate. The magnetic intensity of the area ranges from -74.72 nT to 147.24 nT. The area is marked by the high (pink colour) and low (blue colour) magnetic signatures. The variation in magnetic intensity could be as a result of degree of strike, variation in depth, difference in magnetic susceptibility, difference in lithology, dip and plunge.

The total magnetic intensity data was projected 500 m above the original datum plane. The upward continuation of the total magnetic field intensity (TMI) map is shown in Figure 4. The magnetic intensity of the area ranges from a minimum value of -65.82 nT to a maximum value of 137.95 nT as shown in the upward continuation map (Figure 4).

Figure 5 shows the reduction to pole of the upward continuation of the TMI grid. The magnetic intensity of the area ranging from -136.13 to 227.73 nT was obtained

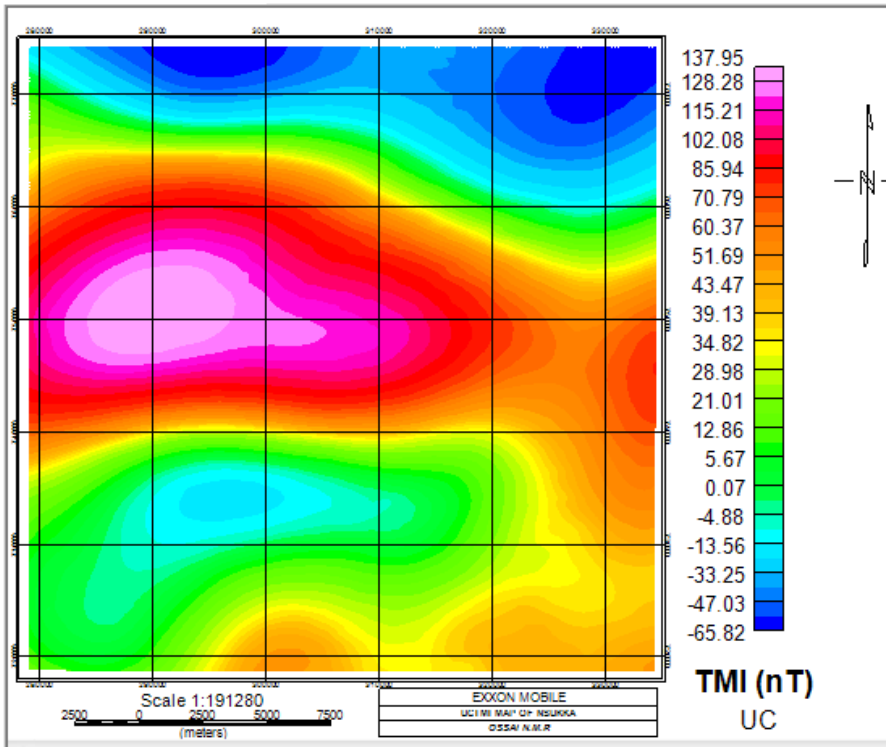

Figure 4. Upward continuation (UC) map and legend of the study area.

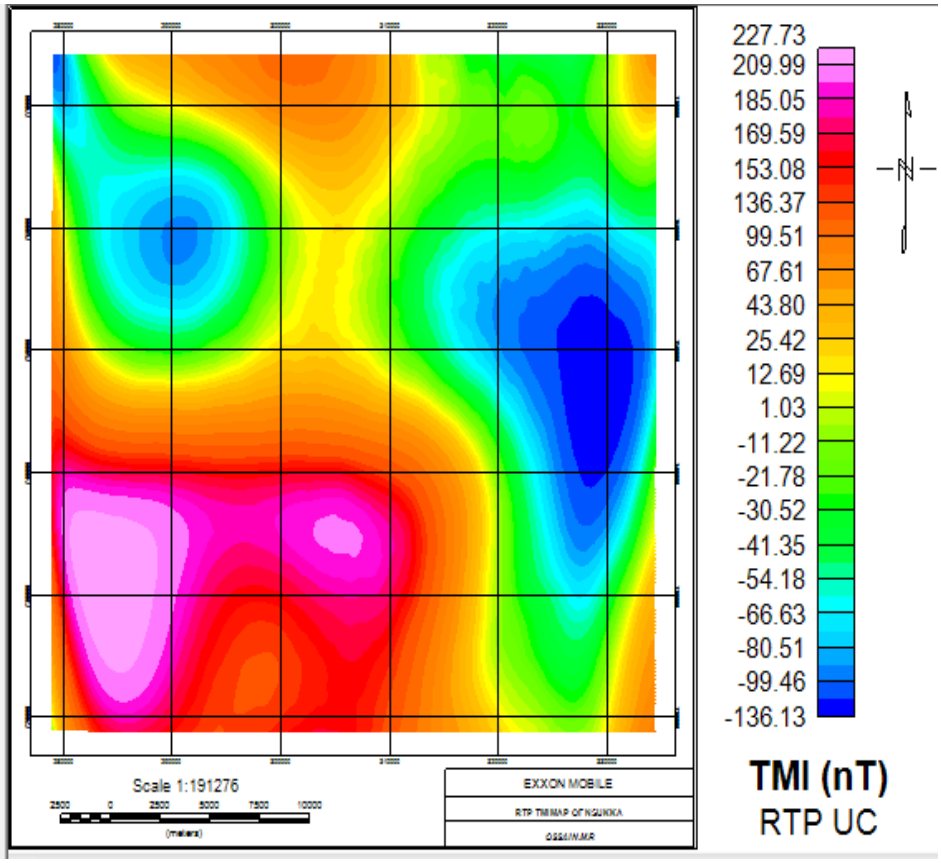

Figure 5. Reduction to pole (RTP) map and legend of the study area.

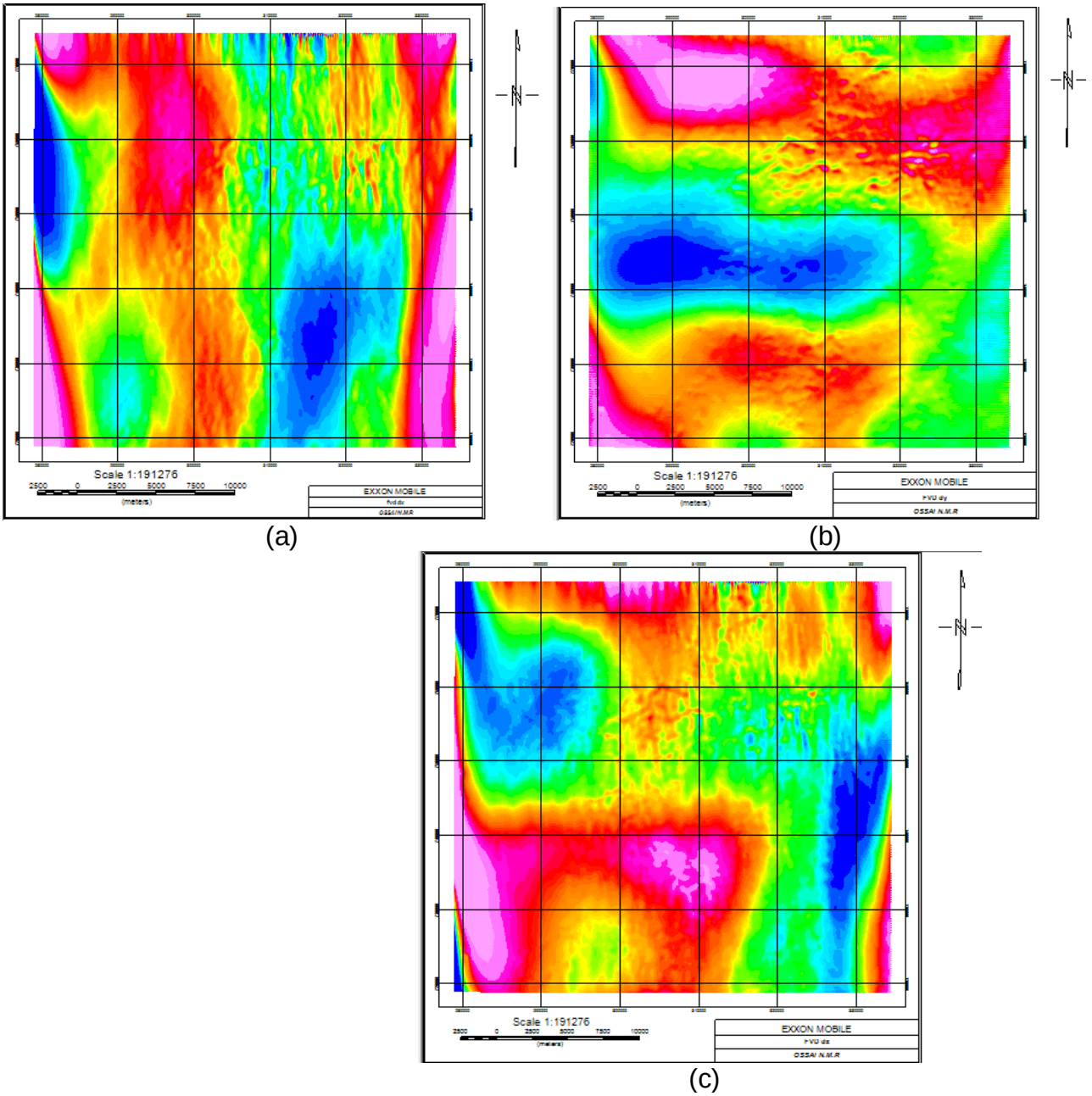

Figure 6. First vertical derivative maps (a) x-direction, (b) y-direction and (c) z-direction.

after reducing the upward continuation (UC) TMI map to magnetic pole. The filtered TMI grid was used for quantitative interpretation of depths to magnetic anomalies.

In computing the SPI depth of magnetic data, Oasis Montaj software was employed. Using the first vertical derivatives and horizontal gradient, the SPI depth was computed. Different magnetic depths and susceptibilities contrast within the study area are indicated by the gridded SPI depth map and legend. Figure 6 (derivative grids) shows that the magnetic bodies are not restricted to a particular location. In Figure 7, the negative depth values shown in the SPI legend depicts the depths of buried magnetic bodies, which may be deep seated basement rocks or near surface intrusive while the positive values depicts outcropping magnetic bodies. The pink colour generally indicates areas occupied by shallow magnetic bodies, while the blue colour depicts areas of deep lying magnetic bodies ranging from -379.43 to -3082.7 m. SPI depth result generally ranges from 151.6 m (outcropping and shallow magnetic bodies) to -3082.7 m (deep lying magnetic bodies).

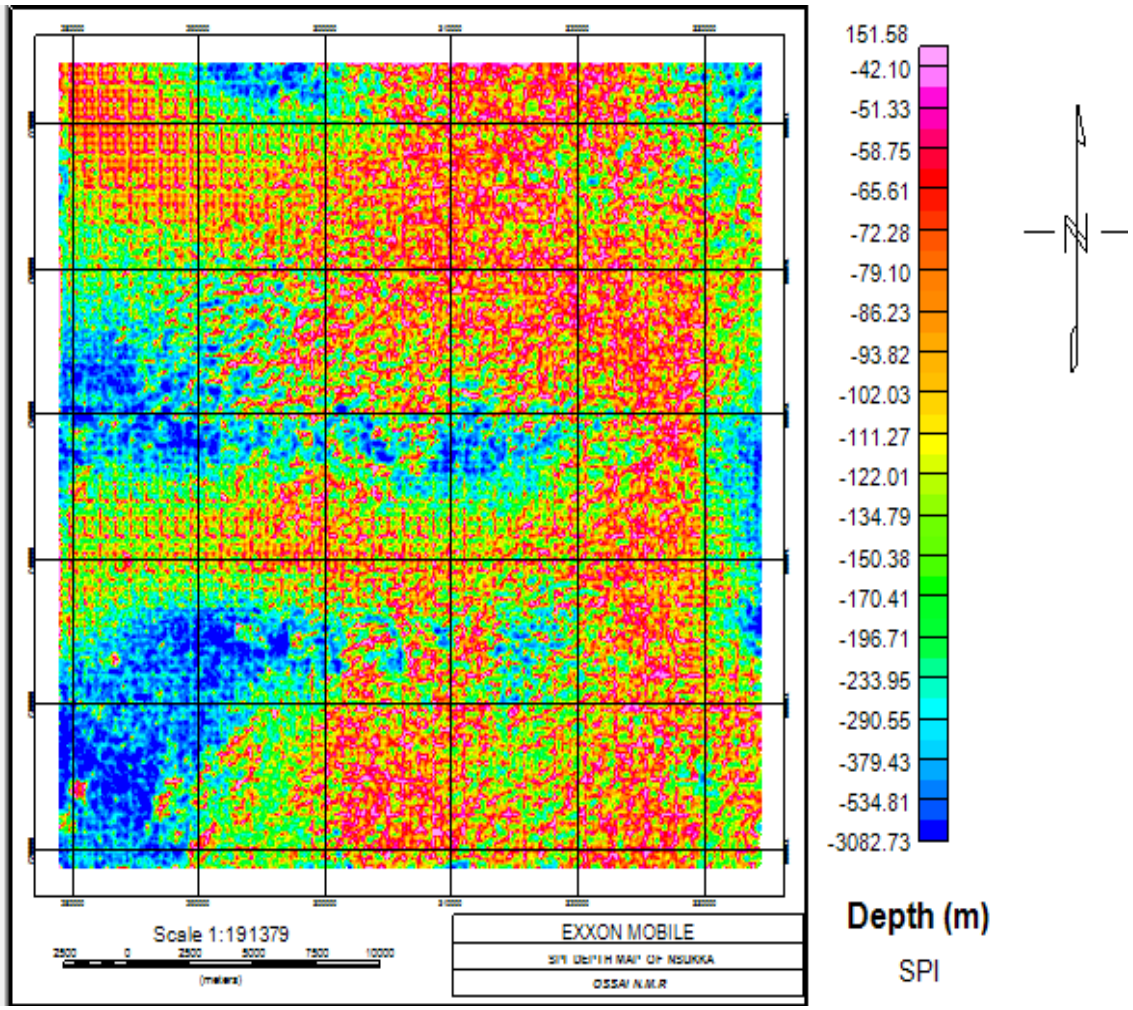

Figure 7. SPI depth map and legend of the study area.

In computing the Euler depth and to produce the Euler depth map and legend, Standard Euler deconvolution (Euler 3-D) interpretation was carried out in three dimensions by employing Oasis montaj software. For four different stuctural index (SI = 0.5, 1, 2, 3), four Euler 3D maps were generated as shown in Figure 8(a, b, c, d). There is no Euler solution (depth) for the particular structural index used as indicated by the areas in the maps without magnetic signatures or colour (depth). The pink colour indicates shallow magnetic bodies, while the blue colour indicates deep lying magnetic bodies (Figure 8). Depths to lateritic bodies and outcrops in the study area that are magnetic because they contain ironstone are signified by positive depth values, while the negative depth values are depths of shallow magnetic bodies below the datum plane

The Euler 3D depth grid for structural index 0.5, 1, 2, and 3 is shown in Figure 8. Depth ranges for SI = 0.5 is from 9.47 to 124.02 m; for SI = 1, depth ranges from 22.51 to 125.29 m; for SI = 2, depth ranges from 39.05 to 120.30 m; and for SI = 3, depth ranges from 7.99 to 128.93 m. The Euler depths were estimated using vertical derivatives in three dimension (x, y, z). Vertical derivatives enhances shallow magnetic bodies. Hence, depths of shallow magnetic bodies or anomalies for different structural index are displayed by Euler method.

Using a single component data (TMI) for multiple bodies, the inversion procedure was performed. The geographic coordinates (*X*, *Y* and *Z*) at which the software (Potent Q) calculated the field due to the model were provided by the data points in the sample of observed data. They further provided the observed field values against which the calculated field values were compared. The root mean square (RMS) difference between the observed and calculated field values was attempted to be minimized by the inversion algorithm. At the end of the inversion, the RMS value was displayed. The RMS value decreased as the fit between the observed and calculated field continues to improve, until a reasonable inversion result was achieved. Less than

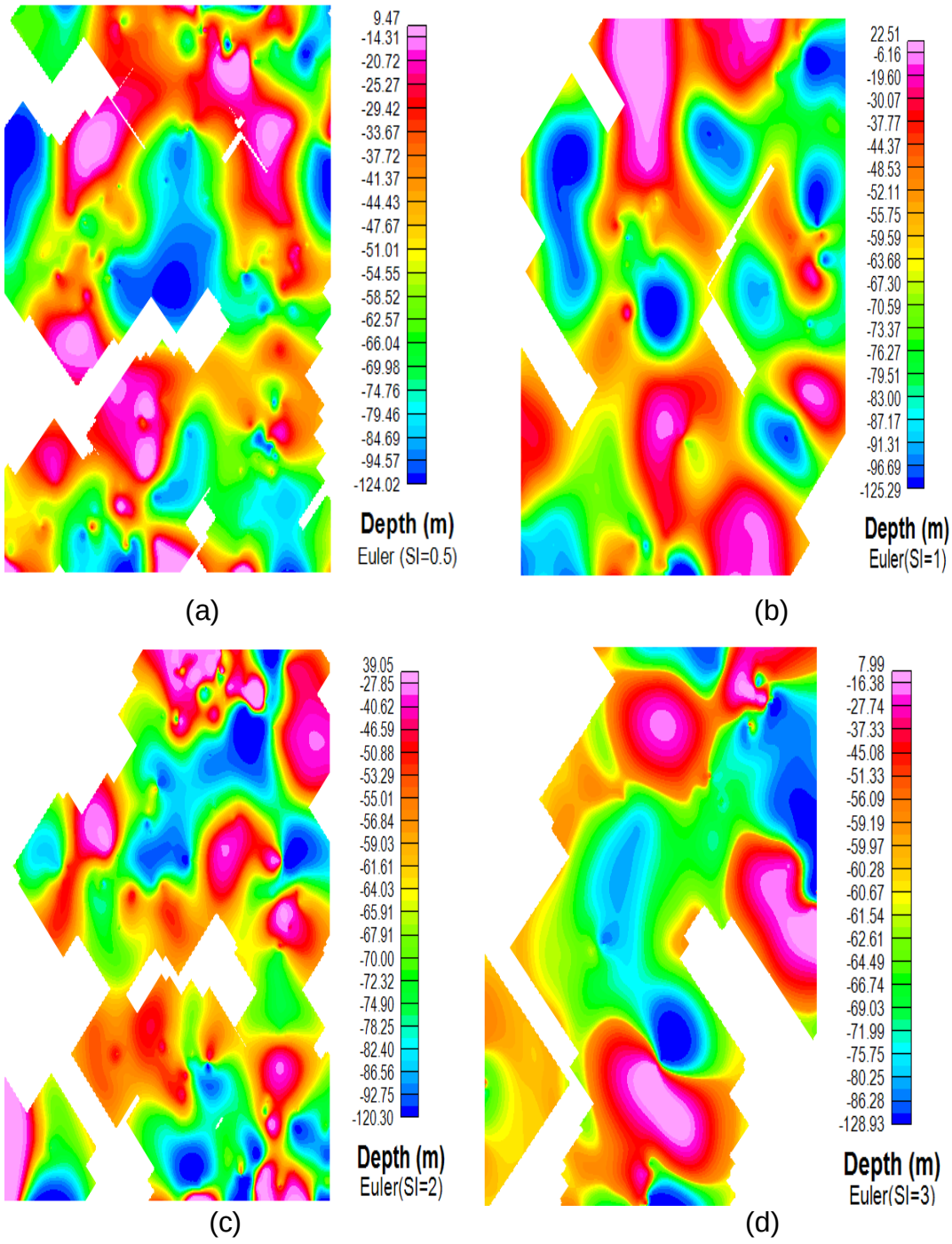

Figure 8. Euler 3D depth grid and legend (a) SI=0.5; (b) SI=1; (c) SI=2 and (d) SI=3.

5% of root mean square value was set as an acceptable error margin.

Five profiles were taken in this modeling and each profile was expected to have a degree of strike, dip and plunge where the observed values matched well with the calculated values. The blue curves in Figure 10 (a, b, c, d, e) represent the observed field values while the red curves represent the calculated field values. The forward modeling being a trial and error method, the shape, position and physical properties of the model were adjusted in order to obtain a good correlation between the calculated field and the observed field data. Using potent software, the field of the model was then calculated. Five bodies were modeled and using the

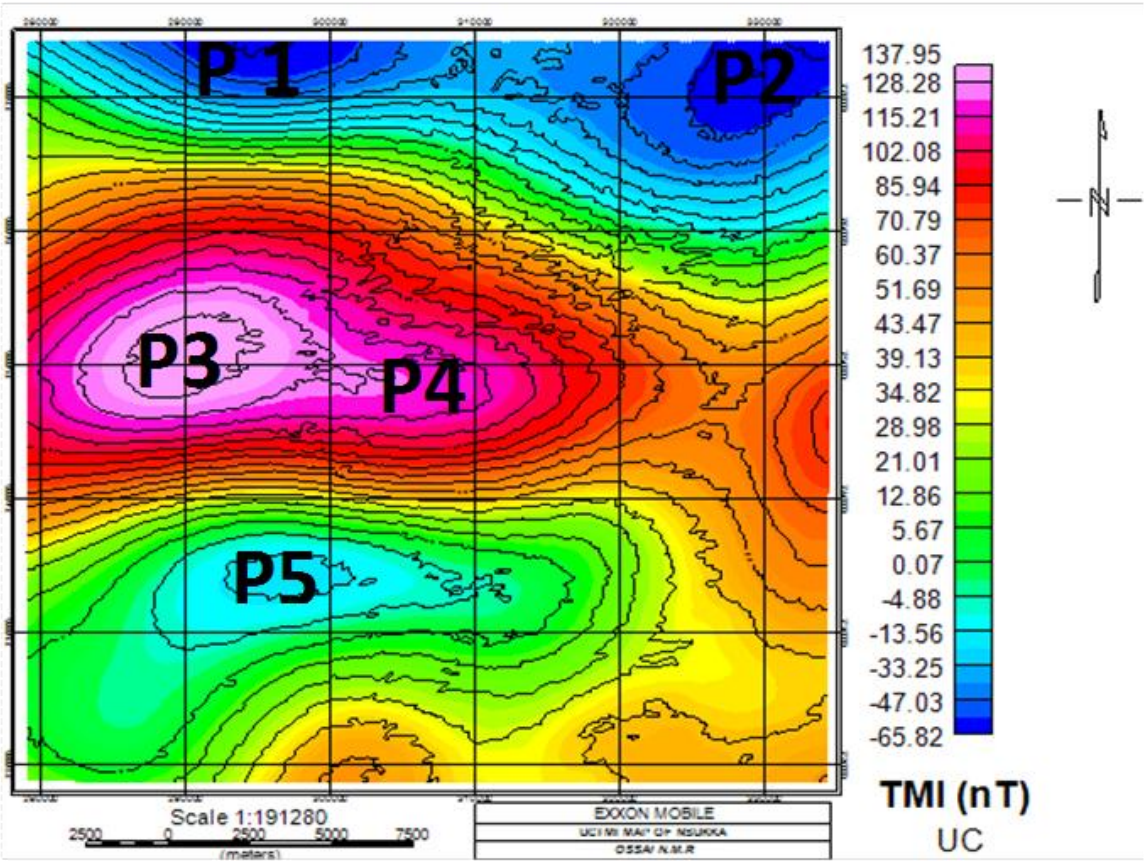

Figure 9. Upward continuation TMI contoured map showing five profiles.

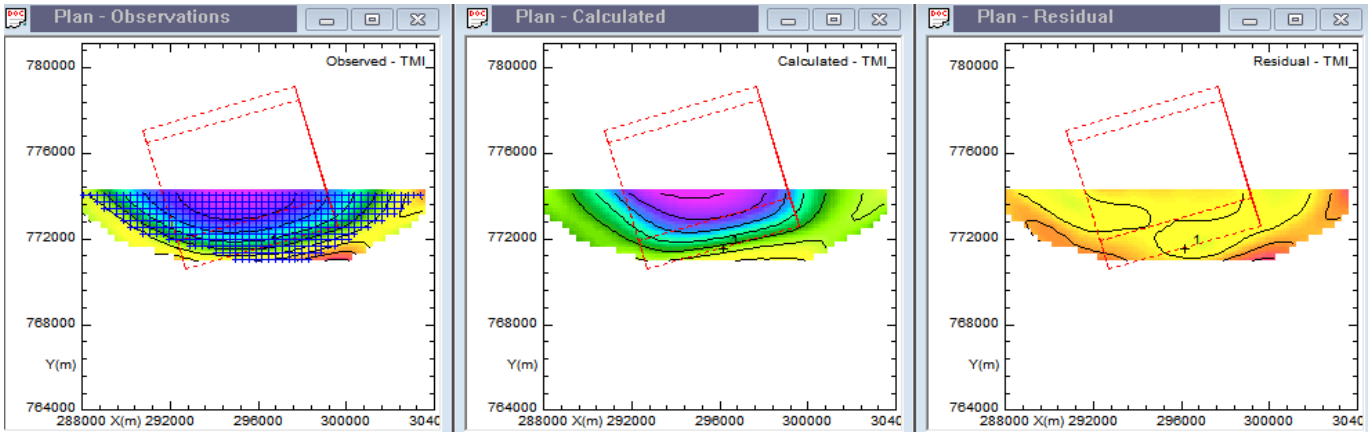

Figure 10a. Subset of profile 1.

upward continuation TMI dataset, inversion method was performed. The potent software used geographic coordinates x, y and z provided by the TMI grid with the field values of the observed field to compare the calculated field values. The difference between the calculated and observed field values is represented by a root mean square value (RMS) which is displayed at the end of each inversion. The RMS value is less than 5% in the inversion model which helped in getting an improved result and match between the observed and calculated field. The five model profiles taken from the upward continuation TMI grid (Figure 9) are shown in Figure 11 (a, b, c, d, e). The shape of the body causing the anomaly is a sphere and its measurement was given in

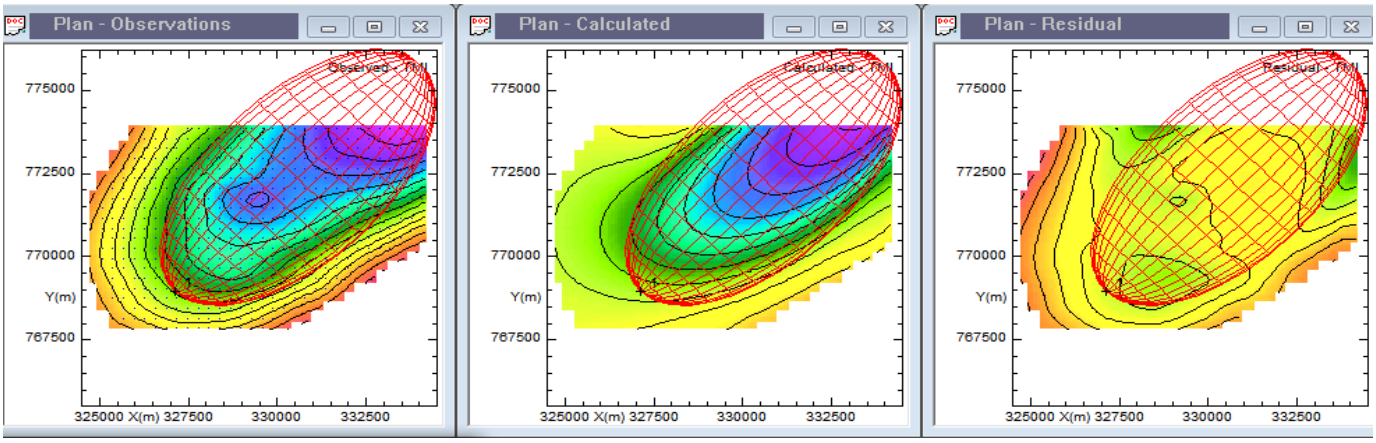

Figure 10b. Subset of profile 2.

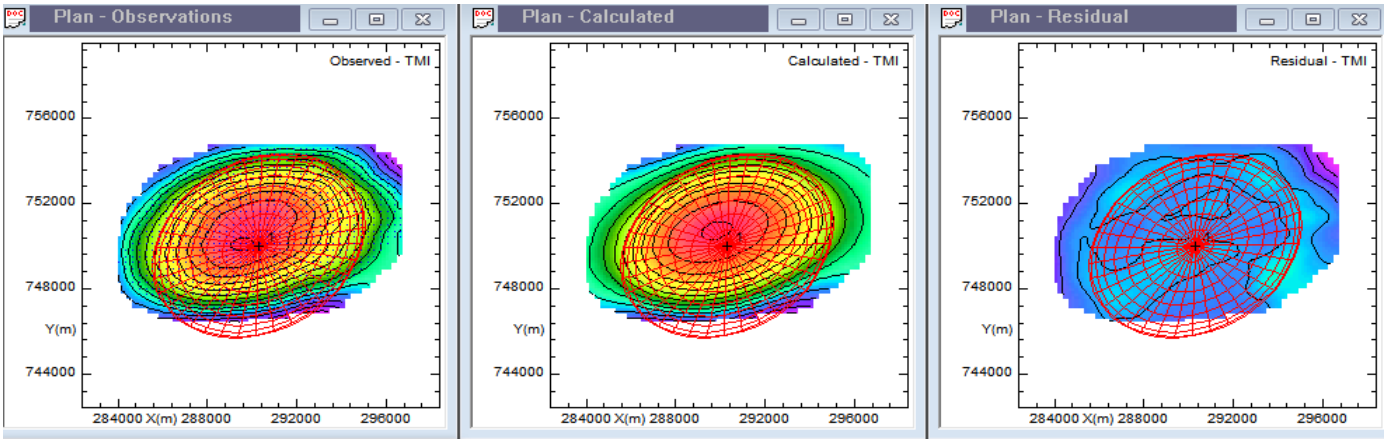

Figure 10c. Subset of profile 3.

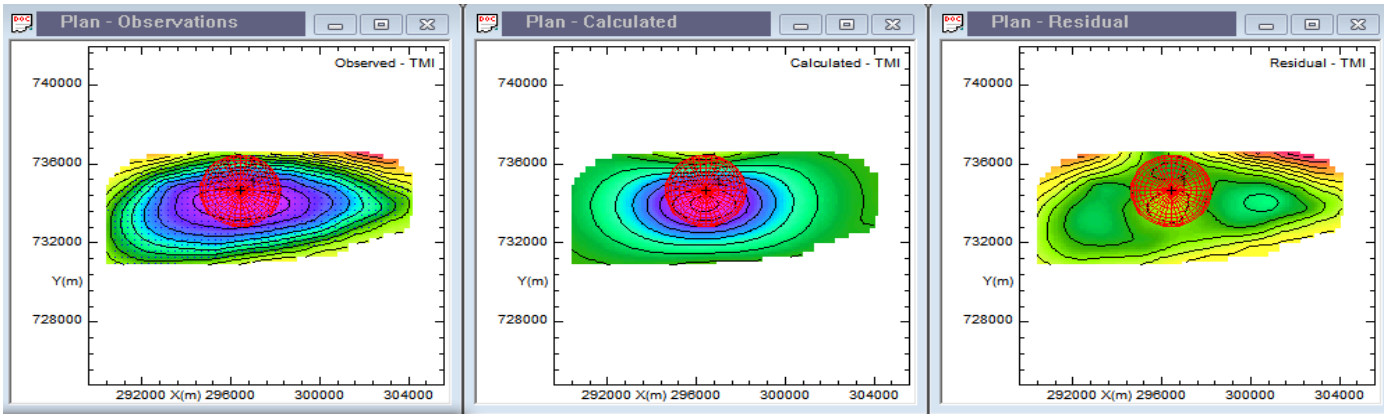

Figure 10d. Subset of profile 4.

terms of radius (3610 m) as shown in the model profile in Figure 11d. Therefore, its ambiguous values of length and height were not considered. The results of the forward and inverse modeling are summarized in Table 1.

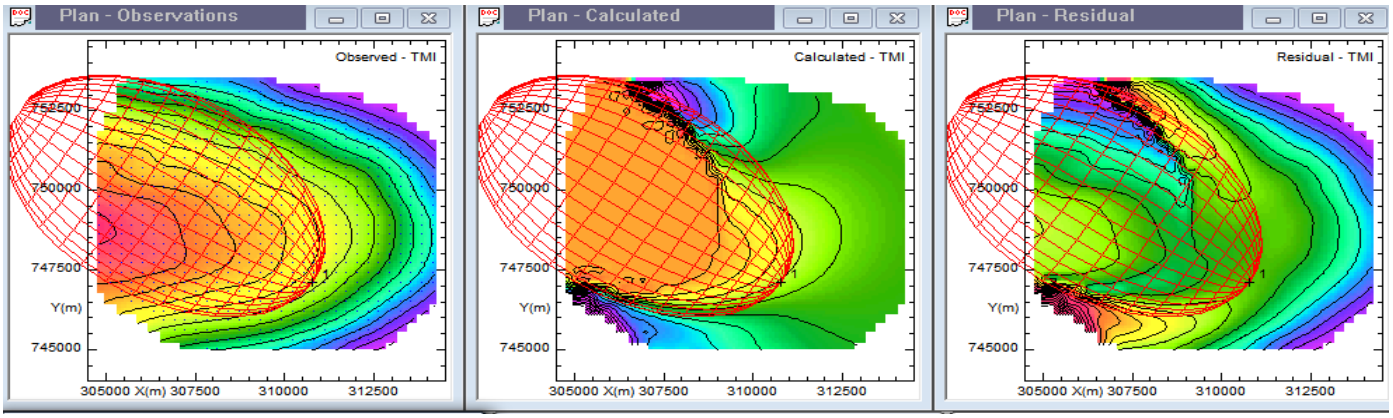

Figure 10e. Subset of profile 5.

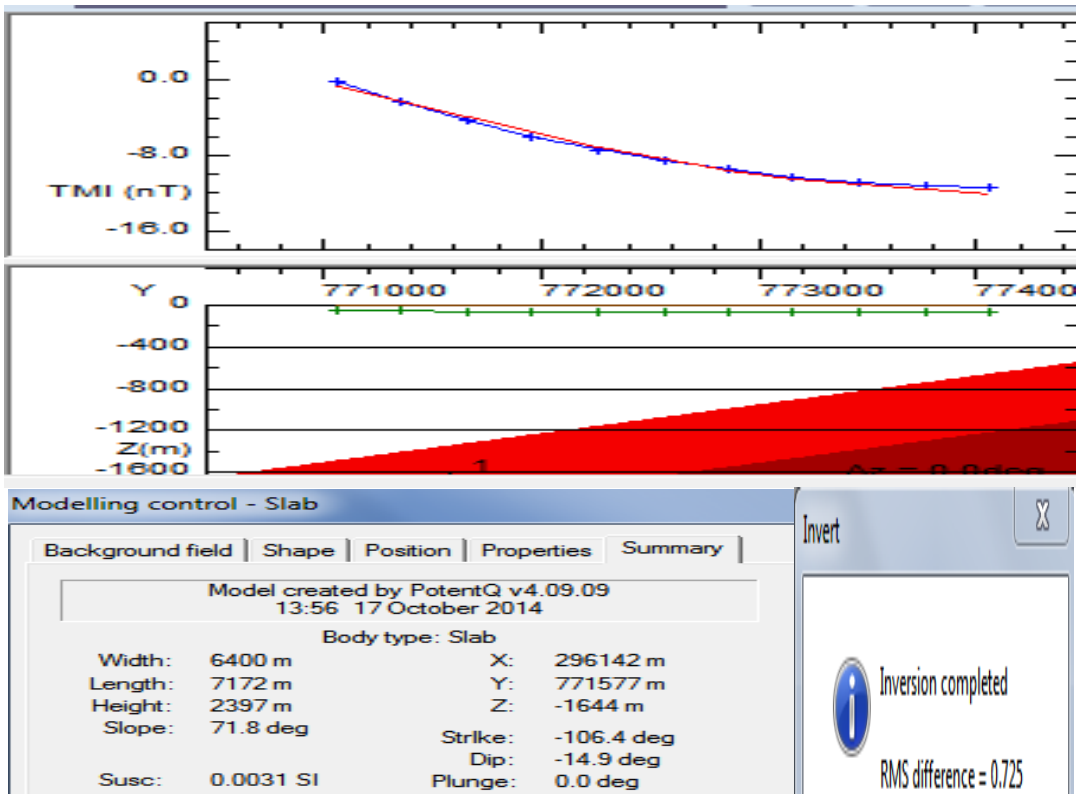

Figure 11a. Model for profile 1.

The susceptibility values obtained from the model profiles 1, 2, 3, 4 and 5 are 0.0031, 0.0073, 1.4493, 0.0069 and 0.0016 respectively, with respective depths of 1644, 2285, 1972, 2193 and 1200 m. Dominance of iron rich minerals like limonite, haematite, pyrrhotite and pyrite are indicated by the susceptibility values and are typically sandstones and ironstones or oxides of iron which are magnetic in nature. Table 2 shows the average magnetic susceptibilities of some mineral (Telford et al., 1990).

DISCUSSION

The depths estimated for shallow magnetic bodies and deep lying magnetic bodies using Standard Euler deconvolution, source parameter imaging (SPI) and forward and inverse modeling methods are within the same range. The depths deduced from the forward and inverse modeling are 1644, 2285, 1972, 2193 and 1200 m for profiles 1, 2, 3, 4 and 5 respectively (Figure 11a, b,

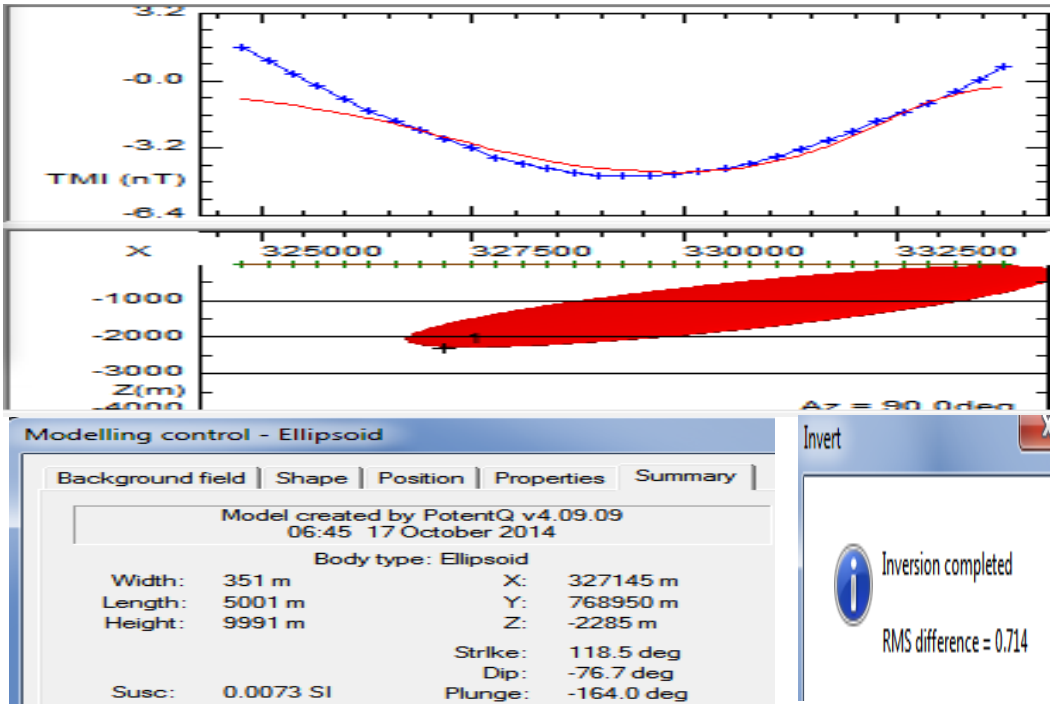

Figure 11b. Model for profile 2.

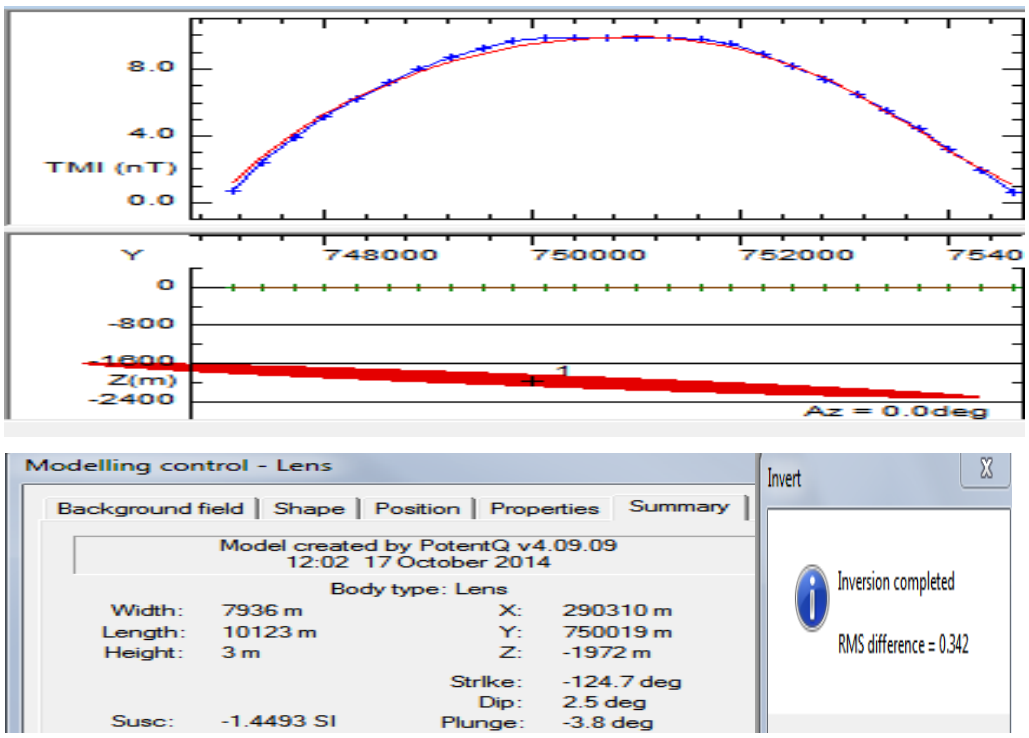

Figure 11c. Model for profile 3.

c, d and e). The susceptibility values obtained from the model profiles 1, 2, 3, 4 and 5 are 0.0031, 0.0073, 1.4493, 0.0069 and 0.0016 respectively. These susceptibility values indicate dominance of iron rich

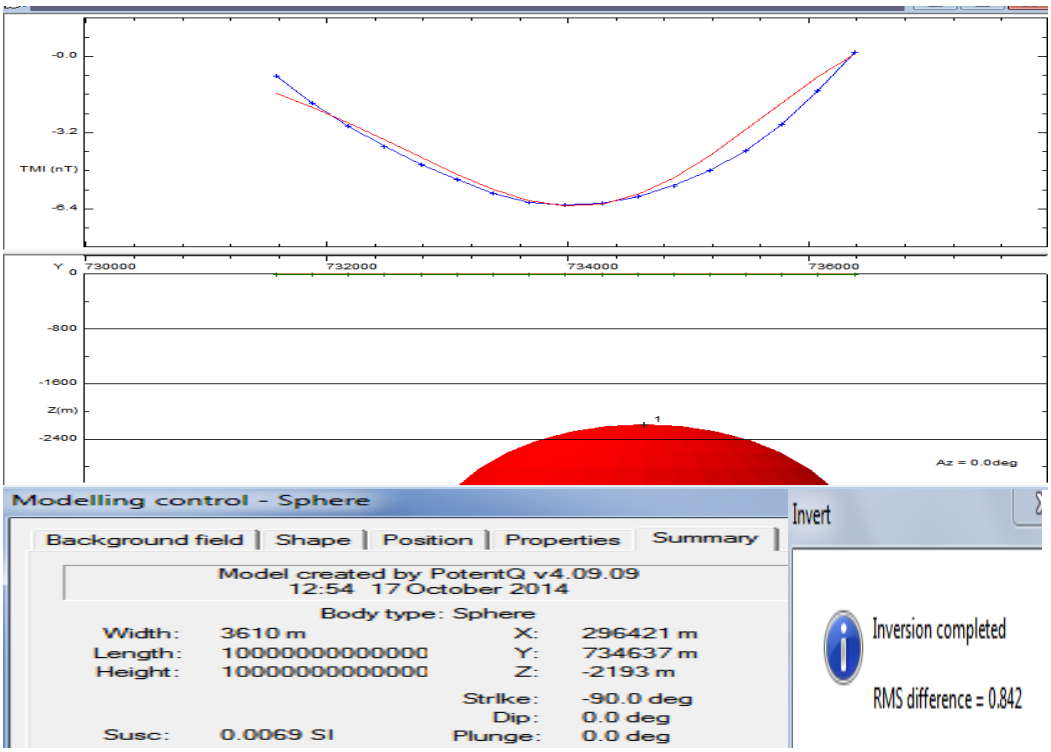

Figure 11d. Model for profile 4.

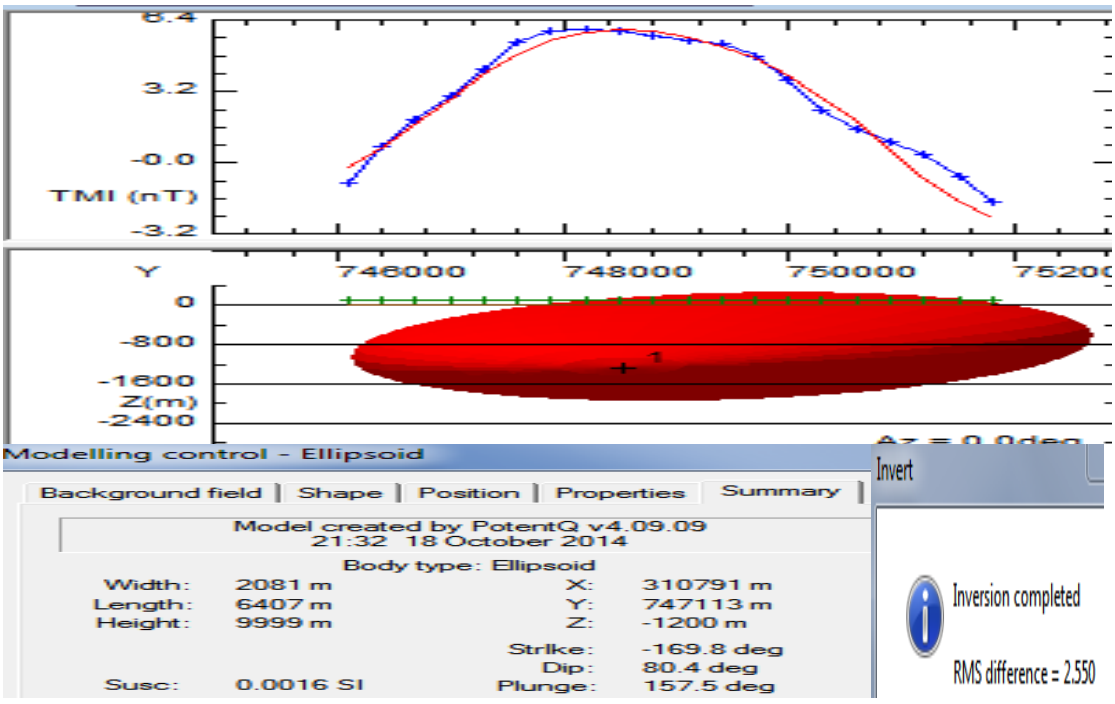

Figure 11e. Model for profile 5.

minerals like limonite, hematite, pyrrhotite and pyrite, and are typically sandstones and ironstones or oxides of iron which are magnetic in nature. The result of SPI depth ranges from 151.6 m (outcropping and shallow magnetic bodies) to -3082.7 m (deep lying magnetic bodies). The depth for shallow magnetic materials ranged from 42.10

Table 1. Summary of Forward and Inverse modeling results.

.

Model	X(m)	Y(m)	Depth (m)	Dip (deg)	Plunge (deg)	Strike (deg)	Body shape	K value (SI)	Possible mineral
1	296142	771577	1644	-14.9	0.0	-106.4	Slab	0.0031	(sandstone) Quartzite
2	327145	768950	2285	76.7	-164.0	118.5	Ellipsoid	0.0073	(ironstone) Hematite
3	290310	750019	1972	2.5	-3.8	-124.7	Lens	1.4493	(ironstone) Pyrrhotite
4	296421	734637	2193	0.0	0.0	-90.0	Sphere	0.0069	(ironstone) Hematite
5	310791	747113	1200	80.4	157.5	-169.8	Ellipsoid	0.0016	(ironstone) Limonite, Pyrite

Table 2. Magnetic susceptibilities of some mineral (Telford et al., 1990).

Rocks	Average magnetic suceptibility (SI)
Dolomite	0.00012
Lime Stone	0.00031
Sands Stone	0.00038
Shale	0.00063
Amphibolite	0.00075
Schist	0.00126
Quartzite	0.00440
Slate	0.00628
Granite	0.00281
Olivine – Diabase	0.02513
Diabase	0.05655
Porphyry	0.06283
Gabro	0.07540
Basalt	0.07540
Diorite	0.08797
Peridotite	0.16336
Acidic Igneous	0.00817

to 79.10 m with an average depth value of 60.6 m and for deep lying magnetic material, depth ranged from 233.95 to 3082.73 m with an average depth value of 1658.34 m. Depth/thickness obtained from modeling results (1200 to 2285 m) and SPI (3082.73 m) show thick sediment that is sufficient for hydrocarbon accumulation which agrees with the work of Wright et al. (1985) that the minimum thickness of the sediment required for the commencement of oil formation from marine organic remains would be 2300 m (2.3 km).

Euler depths for the four different structural index (SI = 0.5, 1, 2, 3) ranges from 9.47 to 128.93 m which are depths of shallow magnetic sources resulting from lateritic bodies in the outcrops within Nsukka area and is within the range of depth for shallow magnetic source bodies as estimated using SPI method. Depths of 35 to 150 m as obtained in this work are good potential water reservoirs in Nsukka area. This is consistence with the assertion of Anomohanran (2013), and Ezeh and Ugwu (2010) that the depth of fresh and good quality aquifer reservoirs in Nsukka area is from 33 to 150 m.

Comparison with some aeromagnetic studies carried out in the Lower Benue Trough

Comparing the results obtained in this work with the results obtained by other researchers in the Lower Benue Trough, Onwuemesi (1997) evaluated the depth to the basement (sedimentary thickness) in the Anambra Basin to vary from 0.9 to 5.6 km. His depth is slightly higher than the depths obtained from this study. Igwesi and Umego (2013) obtained a two layer source model with depth for deeper magnetic source ranging from 1.16 to 6.13 km with average of 3.03 km and depth to the shallower magnetic source ranging from 0.016 to 0.37 km with average of 0.22 km. Their estimated depth agrees with the depth estimated from this study especially within the shallow source. Onu et al. (2011) estimated that the depths to the magnetic source bodies in the lower Benue Trough and some adjoining areas vary from 0.518 to 8.65 km with a mean depth of 3.513 km (for deeper magnetic source bodies) and 0.235 to 3.91 km with a mean depth of 1.389 km (for shallower magnetic source bodies),

which are greater than the depth estimated from this work. Onuba et al. (2011) estimated the depth to basement over Okigwe areas and established two depth models varying from 2.18 to 4.91 km for deeper sources while the shallower sources vary from 0.55 to 1.82 km. However, they did not recommend hydrocarbon exploration in the area since the area has low thickness of sediments on the average. Adetona and Abu (2013) estimated the thickness of sedimentation within the Lower Benue Basin and Upper Anambra Basin by employing spectral depth analysis and obtained a depth of 7.3 km and source parameter imaging to obtain a depth of 9.847 km. This result is also greater than our result. Ezema et al. (2014) estimated maximum depths of 4.96 to 9.8 km and minimum depths of 0.12 to 0.17 km over Abakaliki area. Their estimated depth agrees with our depth for the shallow source. The results of some of these works agree with the results of the present study especially within the shallow source. It should be noted that none of these works were carried out in Nsukka and its environs, but in other parts of Lower Benue Trough.

Conclusion

Interpretation of aeromagnetic data of Nsukka area has been done qualitatively and quantitatively. Source parameter imaging (SPI), standard Euler deconvolution and forward and inverse modeling methods were employed in quantitative interpretation. The estimated depths from the forward and inverse modeling method are 1644, 2285, 1972, 2193 and 1200 m for profiles 1, 2, 3, 4, 5 (Figure 11a, b, c, d and e) respectively. The susceptibility values obtained from the model profiles 1, 2, 3, 4 and 5 are 0.0031, 0.0073, 1.4493, 0.0069 and 0.0016 respectively which indicate dominance of iron rich minerals like limonite, hematite, pyrrhotite, and pyrite and forms lateritic caps on sandstones. Depth result from SPI ranges from 151.6 m (outcropping and shallow magnetic bodies) to -3082.7 m (deep lying magnetic bodies). Sediment thickness of 1644 m to 3082.7 m is sufficient for hydrocarbon accumulation. This agrees with the work of Wright et al. (1985) which asserts that the minimum thickness of the sediment required for the commencement of oil formation from marine organic remains would be 2300 m (2.3 km). From Euler depth results, the depth of contact body ranges from 9.47 m to 124.02 m for SI = 0.5; depth of dyke, silt and thin sheet body ranges from 22.51 m to 125.29 m for SI = 1; depth of line source body ranges from 39.05 m to 120.30 m for SI = 2; and the depth of spherical and compact body like ellipsoid ranges from 7.99 m to 128.93 m for SI = 3. Depths of shallow magnetic sources resulting from lateritic bodies in the outcrops within the study area ranges from 9.47 to 128.93 m (Euler depth for the four different structural index) and is within the range of depth for shallow magnetic source bodies as estimated using SPI method. 35 to 150 m depths are good potential water reservoirs (Anomohanran, 2013; Ezeh and Ugwu, 2010) within Nsukka area. The depths obtained in this work fairly agrees with the depths estimated by many previous researchers (Ofoegbu, 1984; Onwumesi, 1997; Onu et al., 2011; Onuba et al., 2011; Igwesi and Umego, 2013; Adetona and Abu, 2013; Ezema et al., 2014) in lower Benue Trough and Anambra Basin in which Nsukka area falls. Results from SPI and modeling techniques show that Nsukka area has sufficiently thick sediments suitable for hydrocarbon accumulation. This study is a case study which provides a good example of the use of aeromagnetic data for basinal studies in a structurally complex mineral rich Basin.

Conflict of Interest

The authors have not declared any conflict of interest.

ACKNOWLEDGEMENTS

The authors are grateful to Dr. J. U. Chukudebelu of Physics and Astronomy Department and Dr. Andrew I. Oha of Geology Department, University of Nigeria, Nsukka, for their valuable contributions. The authors appreciate the good works of the Editor and the reviewers.

REFERENCES

Adetona AA, Abu M (2013). Investigating the structures within the Lower Benue and upper Anambra Basins, Nigeria, using First Vertical Derivative, Analytical Signal and (CET) Center for Exploration Targeting Plug-in. Earth Sci. 2(5):104–112.

Anomohanran O (2013). Geophysical investigation of groundwater potential in Ukelegbe, Nigeria. J. Appl. Sci. 13(1):119–125.

Ezeh CC, Ugwu GZ (2010). Geoelectrical sounding for estimating groundwater potential in Nsukka L.G.A. Enugu State, Nigeria. Int. J. Phys. Sci. 5(5):415–420.

Ezema PO, Eze ID, Ugwu GZ, Abudullahi UA (2014). Hydrocarbon and Mineral Exploration in Abakaliki, Southeastern Nigeria. Int. J. Eng. Sci. 3(1):24–30.

Igwesi ID, Umego NM (2013). Interpretation of aeromagnetic anomalies over some parts of lower Benue Trough using spectral analysis technique. Int. J. Sci. Technol. Res. 2(8):153–165.

Nwachukwu SO (1972). The tectonic evolution of the southern portion of the Benue Trough, Nigeria. J. Min. Geol. 11:45-55.

Nwajide CS, Reijers TJA (1995). Sedimentology and sequence stratigraphy of selected outcrops in the upper cretaceous of lower Tertiary of the Anambra Basin. SPDC Exploration Report, XPMW 96007:21–37.

Ofoegbu CO (1984). Interpretation of aeromagnetic anomalies over the lower and middle Benue Trough of Nigeria. Geophys. J. R. Astr. Soc. 79:813–823.

Ofoegbu CO (1985). A review of the geology of the Benue Trough, Nigeria. J. Afr. Earth Sci. 3:293-296.

Okeke FN (1992). Comparison of graphical methods of interpretation based on the interpretation of aeromagnetic anomaly profile across the Benue Trough. Nig. J. Phys. 4:103-113.

Onu NN, Opara AI, Oparaku OI (2011). Geological interpretation of the aeromagnetic data over the lower Benue Trough and some adjoining areas. 47th Annual International Conference of Nigerian Mining and Geoscience Society (NMGS), Programmes and Book of Abstracts. P. 43.

Onuba LN, Audu GK, Chiaghanam OI, Anakwuba EK (2011). Evaluation of aeromagnetic anomalies over Okigwe area, Southern Nigeria. Res. J. Environ. Earth Sci. 3(5):498–507.

Onwuemesi AG (1997). One dimensional spectral analysis of aeromagnetic anomalies and curie depth isotherm in Anambra Basin of Nigeria. J. Geodynamics. 23(2):95-107.

Onwuemesi AG (1995). Interpretation of magnetic anomalies from the Anambra Basin of southeastern Nigeria. Ph.D thesis, Nnamdi Azikiwe University, Awka, Nigeria.

Petters SW (1978). Stratigraphic Evolution of the Benue Trough and its implications for the Upper Cretaceous Paleogeography of West Africa. J. Geol. 86(3):11-322.

Reid AB, Allsop JM, Granser A, Millett AJ, Somertom IW (1990). Magnetic interpretation in three dimension using Euler deconvolution. Geophysics. 55:80–91.

Revees C (2005). Aeromagnetic Surveys; Principles, Practice and Interpretation. GEOSOFT.

Telford WM, Geldart LP, Sheriff RE (1990). Applied Geophysics 2nd edition. Cambridge University Press, Cambridge.

Thompson DT (1982). EULDPH- new technique for making computer assisted depth estimate of magnetic data. Geophysics. 47:31–37.

Ugbor DO, Okeke FN (2010). Geophysical investigation in the lower Benue Trough of Nigeria, using gravity method. Int. J. Phys. Sci. 5(11):1757–1769.

Ugwu GZ, Ezema PO (2012). Forward and inverse modeling of aeromagnetic anomalies over Abakaliki and Nkalagu areas of the Lower Benue Trough, Nigeria. Int. Res. J. Geol. Mining. 2(8):222–229.

Ugwu GZ, Ezema PO, Ezeh CC (2013). Interpretation of aeromagnetic data over Okigwe and Afikpo areas of lower Benue Trough, Nigeria. Int. Res. J. Geol. Mining. 3(1):1–8.

Wright JB (1976). Origins of the Benue Trough – a critical review. In: Geology of Nigeria, eds. Kogbe CA. Elizabethan Publ. Co. Lagos. pp. 309-318.

Wright JB, Hastings D, Jones WB, Williams HR (1985). Geology and Mineral resources of West Africa. George Allen and Urwin, London.

academicJournals

Vol. 10(17), pp. 520-527, 16 September, 2015
DOI: 10.5897/IJPS2015.4404
Article Number: DED6A6955497
ISSN 1992 - 1950
Copyright ©2015
Author(s) retain the copyright of this article
http://www.academicjournals.org/IJPS

International Journal of Physical Sciences

Full Length Research Paper

Ab-initio calculations of magnetic behavior in wurtzite $Al_xV_{1-x}N$ compound

Miguel J. R. Espitia [1]*, John H. F. Díaz [1] and César O. López[2]

[1]Grupo GEFEM, Universidad Distrital Francisco José de Caldas, Bogotá, Colombia.
[2]Grupo Avanzado de Materiales y Sistemas Complejos GAMASCO, Departamento de Física, Universidad de Córdoba, Montería Colombia.

Received 25 August, 2015; Accepted 8 September, 2015

The density functional theory was employed in order to study the structural, electronic, and magnetic properties of the $Al_xV_{1-x}N$ (x=0.25, 0.50, and 0.75) compound in the wurtzite-type structure. The calculations were executed using the method based on pseudopotential, employed exactly as implemented in Quantum ESPRESSO code. For the description of the electron-electron interaction, generalized gradient approximation (GGA) was used. The analysis of the structural properties shows that the lattice constant increases with the concentration of Al atoms, but the functional relations are not linear. The electronic density studies show that the $Al_{0.25}V_{0.75}N$ and $Al_{0.50}V_{0.50}N$ compounds exhibit a half-metallic behavior, while $Al_{0.75}V_{0.25}N$ is metallic. This compound exhibits a ferromagnetic character with a magnetic moment of 2 μ_β/atom-V. The ground-state ferromagnetic behavior essentially comes from the polarization of the V-3d that crosses the Fermi level. These compounds are good candidates for potential applications in spintronics and as spin injectors.

Key words: Density functional theory (DFT), half-metallic ferromagnetism, structural and electronic properties.

INTRODUCTION

AlN stabilizes in the wurtzite (WZ) structure in bulk form (Nakamura et al., 1997). AlN, as the semiconductor material with the largest band-gap has many superior properties and thus is the best material for constructing devices in the violet region, and it is also used as an electronic packaging material, and is applied to optical disks and lithographic photo masks as well (Jonnard et al., 2004; Carcia et al., 1996; Carcia et al., 1997). Aluminium nitride exhibits stability at high temperatures, considerable thermal conductivity, low thermal expansion, and a high resistance to gases and chemicals (Beheshtian et al., 2012). Also, wurtzite AlN has the largest direct band gap, at 6.1 eV, as well as high acoustic velocity, which distinctly opens up the possibility of fabrication of various optical devices in the ultraviolet wave length region and different surface acoustic wave devices. Recently, Group III semiconductors such as AlN have received great attention because of their possible use as diluted magnetic semiconductors and their potential applications in the field of spintronics. For these applications, ferromagnetism at room temperature is a requirement. In recent years, high-temperature ferromagnetism has been reported by many researchers in several types of transition metal (TM)-doped

*Corresponding author. E-mail: mespitiar@udistrital.edu.co
Author(s) agree that this article remain permanently open access under the terms of the Creative Commons Attribution License 4.0 International License

semiconducting nitrides and oxides. Gonzalez et al. (2011) through theoretical studies, predict room-temperature ferromagnetism in p-type Mn-doped GaN (Gonzalez et al., 2011), while Vargas et al. (2015) observed half-metallic ferromagnetism behavior in $Zn_xMn_{1-x}O$ compounds. On the other hand, it has been reported that Sc-, Cr-, Co-, Mn-, Er-, Mg-, Ca- and Cu-doped AlN are ferromagnetic (FM) (Lei et al., 2009; Wu et al., 2007; 2003; Frazier et al., 2003; Yang et al., 2007; Dridi et al., 2011; Wu et al., 2006; Zhang et al., 2008; Huang et al., 2007). But investigations of AlN:V systems are rare, be they theoretical or experimental. For this reason, in this paper the authors present a systematic theoretical study of the structural, electronic and magnetic properties of the $Al_xV_{1-x}N$ compound.

COMPUTATIONAL METHODS

The calculations were carried out within the framework of density functional theory (DFT), as implemented in the Quantum ESPRESSO software package (Giannozzi et al., 2009). The exchange and correlation effects of the electrons were dealt with using the generalized gradient approximation (GGA) of Perdew, Burke, and Ernzerhof (PBE) (Perdew et al., 1997). Electron–ion interactions were treated using the pseudopotential method (Vanderbilt, 1990; Laasonen et al., 1993). The electron wave functions were expanded into plane waves with a kinetic energy cutoff of 40 Ry. For the charge density, a kinetic energy cutoff of 400 Ry was used. A 6×6×4 Monkhorst-Pack mesh (Monkhorst and Pack, 1976) was used to generate the k-points in the unit cell. The calculations were performed taking into account the spin polarization. Self-consistency was achieved by requiring that the convergence of the total energy be less than 10^{-4} Ry.

To calculate the lattice constant, the minimum volume, the bulk modulus, and the cohesive energy in the wurtzite structure, calculations were fit to the Murnaghan equation of state (Murnaghan, 1944) (Equation 1):

$$E(V) = E_0 + \frac{B_0 V}{B_0^{'}}\left[\frac{\left(V_0 / V\right)^{B^{'}}}{B_0^{'}-1}+1\right] - \frac{B_0 V_0}{B_0^{'}-1} \quad (1)$$

Where B_0 is the bulk modulus, its first derivative is B'_0, V_0 is the equilibrium volume of the cell, E_0 represents the ground-state total energy and V is the volume of the unit cell.

RESULTS AND DISCUSSION

Structural properties

To determine the structural properties in the ground state, such as the lattice constant (a_0), equilibrium volume (V_0), bulk modulus (B_0), and total energy (E_0) of the binary compounds AlN and VN and of the three allowed ternary compounds, $Al_xV_{1-x}N$ (x=0.25, 0.50, and 0.75), in the wurtzite structure, the total energy was calculated as a function of the volume. The results were fit to the Murnaghan equation of state (Equation 1). Additionally, the total energy variation was calculated as a function of the volume of the ferromagnetic (FM) and antiferromagnetic (AFM) phases in order to find the most favorable magnetic phase of the $Al_xV_{1-x}N$ (x=0.25, 0.50, and 0.75) compounds. In order to calculate the most favorable AFM structure, the authors using various AFM configuration, for this purpose, the supercells of 1×1×1 (for $Al_{0.50}V_{0.50}N$) and 1×1×2 (for $Al_{0.25}V_{0.75}N$ and $Al_{0.75}V_{0.25}N$) were used to get even numbers of V atom for switching spin state up and down. Figure 1 shows the energy-volume curves for $Al_xV_{1-x}N$ (x=0.25, 0.50, and 0.75) compounds in the FM and AFM states. In the ground state, the total energy differences between the FM and AFM states ($\Delta E = E_{FM} - E_{AFM}$) were -0.11, -0.014, and -0.05 eV for x=0.25, 0.50, and 0.75, respectively. In all cases, the FM state was more energetically favorable than the AFM state.

The authors can see that the equilibrium lattice constant a_0 of the binary AlN compound calculated in this paper are in very good agreement with the values reported theoretically and experimentally, since they differ by less than one percent. For the allowed ternary compounds of $Al_xV_{1-x}N$ (x=0.25, 0.50, and 0.75), the structures are obtained by replacing Al atoms with V atoms in the AlN supercell. For x=0.25 and x=0.50, an Al atom is replaced by a V atom in supercells of 8 and 4 atoms, respectively. For x=0.75, three Al atoms are replaced by three V atoms in a supercell of 8 atoms. Figure 2 shows the crystal structure of the allowed ternary compounds, $Al_xV_{1-x}N$ (x=0.25, 0.50, and 0.75), obtained after the structural relaxation; in all cases, the space group obtained is the tetragonal structure p3 m1 (N° 156).

The authors observe that VN has a larger bulk modulus than the AlN, and the bulk modulus of the $Al_xV_{1-x}N$ compound decreases as the concentration Al increases. However, the values of the bulk moduli of the allowed ternary compounds of $Al_xV_{1-x}N$ (x=0.25, 0.50, and 0.75) shown in Table 1 are high, confirming that they are quite rigid, making them good candidates for possible applications in devices operated at high temperature and high power as well as in hard coatings.

Table 1 shows that the equilibrium lattice constant value increases with an increase in the concentration of Al atoms. But the increase in the lattice constant is small, resulted from the minor difference in atomic radius between V (1.34 Å) and Al (1.43 Å). Figure 3 shows the variation of the lattice constant as a function of the Al concentration. It can be observed that the variation in the lattice parameter versus Al composition is nonlinear. A strong deviation from Vegard's law is clearly visible for the equilibrium lattice constants a_0, since there is an upward bowing. This deviation indicates a strong interaction between the ions of V and Al. A similar result was found by Boukra et al. (2010) in their study of

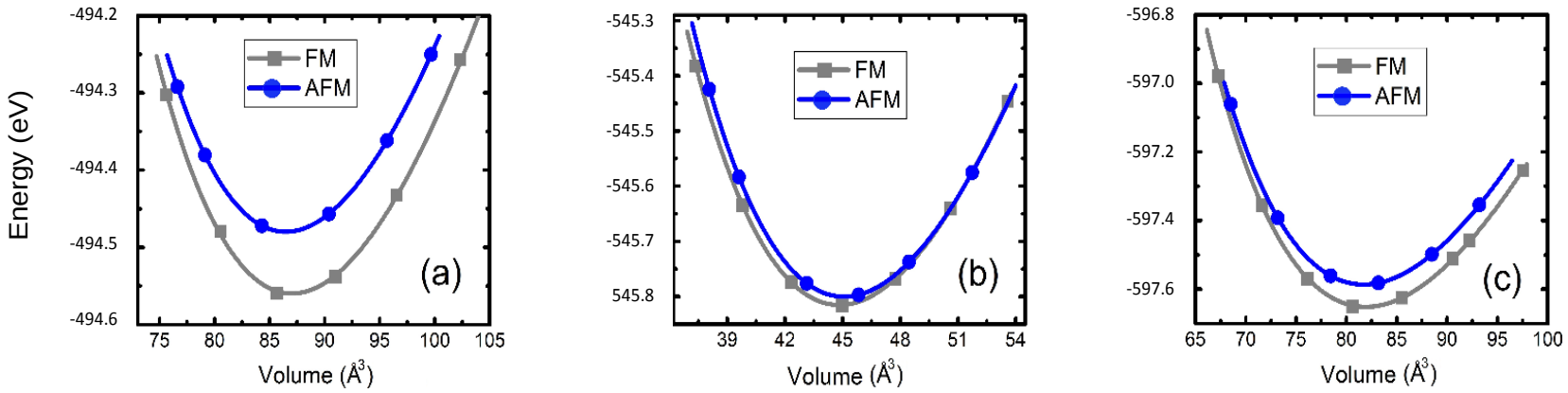

Figure 1. Total energy as a function of volume for (a) $Al_{0.25}V_{0.75}N$, (b) $Al_{0.50}V_{0.50}N$, and (c) $Al_{0.75}V_{0.25}N$ compounds.

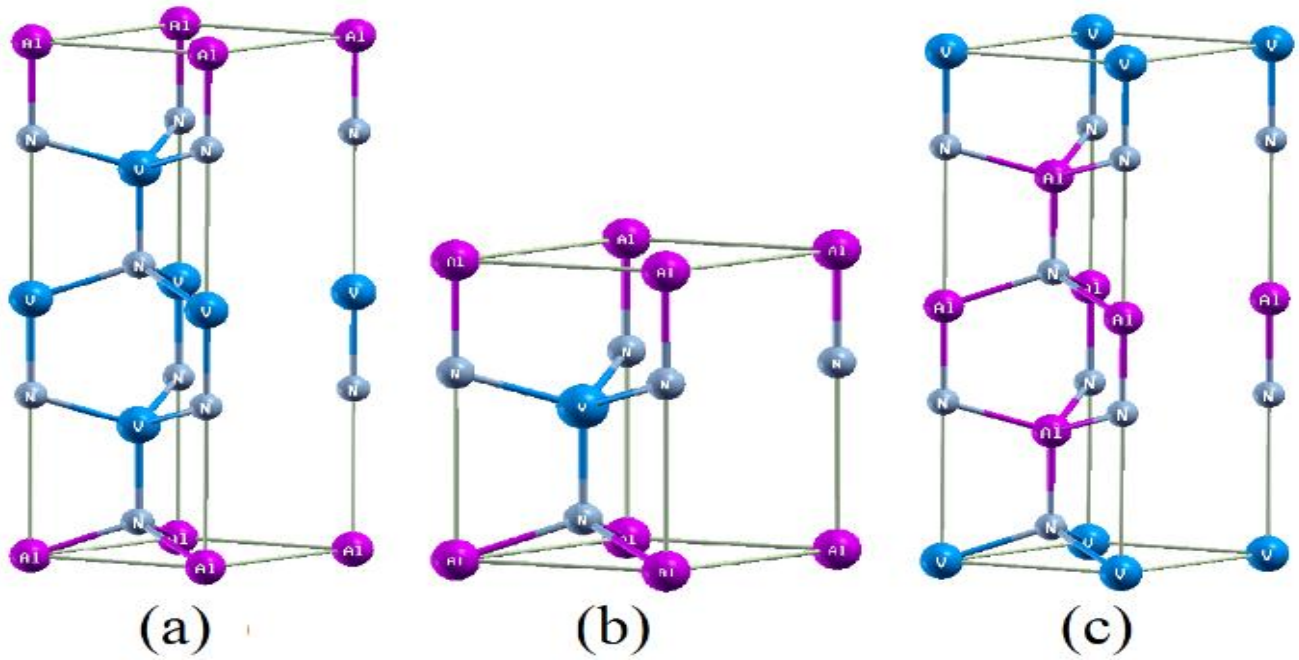

Figure 2. Unit cell of the allowed ternary compounds: (a) $Al_{0.25}V_{0.75}N$, (b) $Al_{0.50}V_{0.50}N$ (c) $Al_{0.75}V_{0.25}N$.

Table 1. Lattice constant (a_0), equilibrium volume (V_0), bulk modulus (B_0), and total energy (E_0) of the binary compounds AlN and VN and of the three allowed ternary compounds, $Al_xV_{1-x}N$ (x=0.25, 0.50, and 0.75), in the wurtzite structure.

Compound	a_0 (Å)	V_0 (Å^3)	B_0 (GPa)	E_0 (eV)
VN	3.092	44.083	232.564	- 648.837
$Al_{0.25}V_{0.75}N$	3.107	81.917	224.544	- 597.140
$Al_{0.50}V_{0.50}N$	3.118	44.828	209.350	- 545.815
$Al_{0.75}V_{0.25}N$	3.126	87.020	198.170	- 494.559
AlN	3.130	42.217	193.450	- 443.331
Other calculations				
VN	3.10[a]	-	209[a]	-
AlN	3.123[b]	-	192[b]	-
	3.111[c]	-	185[c]	-

a (Gonzalez et al., 2007) theoretical, b (Warner et al., 2002) Theoretical, c (Schulz et al., 1997) Experimental

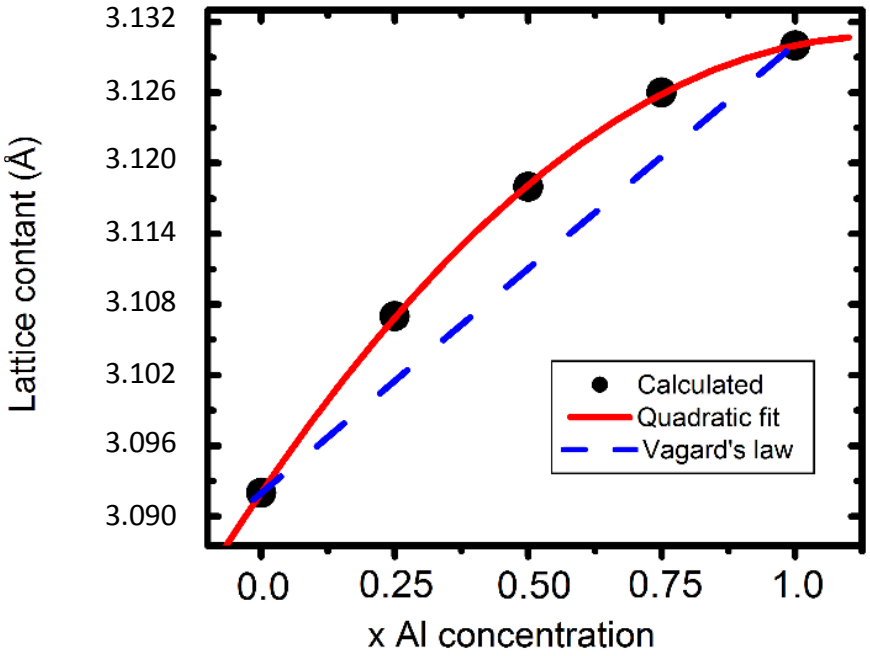

Figure 3. Lattice constant as a function of Al-concentrations.

$Ga_xMn_{1-x}N$ ternary systems using DFT.

In this case, the lattice constant of the $Al_xV_{1-x}N$ (x=0.25, 0.50 and 0.75) ternary compounds seems to obey a quadratic trend. To verify this dependence, the author carried out a fit to a quadratic polynomial and found that the relation between the lattice constant and the concentration x of Al is: $a_{AlxV1-xN}=xa_{AlN}+(1-x)a_{VN}-x(1-x)b$, where a_{AlN} and a_{VN} are shown in Table 1, and b=-0.019 Å.

In order to verify the relative stability of the $Al_xV_{1-x}N$ (x=0.25, 0.50, and 0.75) compounds with reference to the terminal phases, the author calculated the corresponding formation energy, which is expressed as the difference between the total energy of the ternary $Al_xV_{1-x}N$ phases, $E^{phase}_{Al_xV_{1-x}N}$ and of the references states of wurtzite AlN, $E^{wurtzite}_{AlN}$ and NaCl of VN, E^{NaCl}_{VN} (Zhang and Veprek, 2007; Sheng et al., 2008):

$$E_f = E^{phase}_{Al_xV_{1-x}N} - xE^{wurtzita}_{AlN} - (1-x)E^{NaCl}_{VN}$$

Table 2 shows the energy of formation values of the allowed ternary compounds of $Al_xV_{1-x}N$ (x=0.25, 0.50, and 0.75). The E_0 energies of the binary compounds AlN and

Table 2. Energy of formation of the allowed ternary compounds of $Al_xV_{1-x}N$ (x=0.25, 0.50, and 0.75).

Compound	E_f (eV)
$Al_{0.25}V_{0.75}N$	0.320
$Al_{0.50}V_{0.50}N$	0.270
$Al_{0.75}V_{0.25}N$	0.148

VN in their ground states are negative (Table 1). However, according to the results of Table 2, the value of the energy of formation of each ternary compound is positive; therefore, the $Al_xV_{1-x}N$ compounds (x=0.25, 0.50, and 0.75) are metastable. This finding implies that the compounds cannot grow under equilibrium conditions, and therefore it is necessary to supply energy in order to grow them (Zhang and Veprek, 2007; Sheng et al., 2008). The results obtained for the energy of formation is important, because by knowing these values the growth conditions can be improved in order to enable one to grow good-quality $Al_xV_{1-x}N$ compounds (x=0.25, 0.50, and 0.75).

According to the results of Table 2, the smallest value of the energy of formation corresponds to the $Al_{0.75}V_{0.25}N$ ternary compound; therefore, this is the most energetically stable structure. Additionally, the moderate formation-energy values indicate that the compounds can easily be grown experimentally. The fact that $Al_{0.75}V_{0.25}N$ compound has the lowest formation energy can be understood as follows; the ground state energy of the binary compound VN is smaller than the AlN, due that the VN has more electrons. For this reason, Table 1 shows the ground state energy of the ternary compounds $Al_xV_{1-x}N$ increases with increasing the concentration of Al atoms and therefore the energy of formation of the $Al_{0.75}V_{0.25}N$ ternary compound is the most lowest.

Electronic properties

Figures 4a, b, and c show the total density of states (TDOS) and partial density of states (PDOS) of the orbitals that contribute most near the Fermi level of $Al_xV_{1-x}N$ (x=0.25, 0.50, and 0.75) compounds, respectively. The TDOS of the allowed ternary compounds $Al_{0.25}V_{0.75}N$ and $Al_{0.50}V_{0.50}N$ (Figures 4a and b) shows that they are half-metallic and ferromagnetic. This result occurs because in the valence band close to the Fermi level, the majority spins (spin-up) are metallic, and the minority spins (spin-down) are semiconductors. These compounds have a spin polarization of 100% of the conduction carriers in the ground state, which is a requirement for spin injectors (Vargas et al., 2015). This finding suggests that these ternary compounds can be efficiently used as spin injectors. Figure 4c shows the TDOS of the $Al_{0.75}V_{0.25}N$ compound. It is clear that this ternary compound does not exhibit half-metallicity. Since the valence and conduction bands cross the Fermi level, $Al_{0.75}V_{0.25}N$ has a metallic character.

As seen in Figure 4, for the ternary compounds in the valence band near the Fermi level, the spin-up density (the majority spins) is mainly dominated by the V-3d states, with a small contribution of the N-2p states, which cross the Fermi level. Therefore, the magnetic properties of the ternary compounds essentially come from the polarization of the V-3d orbital.

In order to fully understand the mechanism by which the FM state in the $Al_xV_{1-x}N$ (x=0.25, 0.50, and 0.75) compound is stabilized; the authors can explain it with the help of the density of states. It can clearly be seen that when the V atom occupies the position of the Al atom in the wurtzite-type supercell, it introduces new states in the energy gap of the AlN semiconductor, resulting in a half-metallic character for $Al_{0.25}V_{0.75}N$ and $Al_{0.50}V_{0.50}N$ and a metallic one for the $Al_{0.75}V_{0.25}N$ compound. The tetrahedral crystal field of the surrounding N ligands splits the fivefold degenerate V-3d states into two-fold degenerate low-energy e_g(d_{z^2} and $d_{x^2-y^2}$) and three-fold degenerate high-energy t_{2g} (d_{xy}, d_{xz} and d_{yz}) states. The electron configuration of the V atom in the $Al_xV_{1-x}N$ (x=0.25, 0.50, and 0.75) compounds can be attributed to the V^{3+} (Katayama et al., 2003). Therefore, V atoms have three valence electrons {[Ar]$3d^3$}; two electrons occupy the doubly degenerate e_g states and one electron and two holes the triply degenerate t_{2g} state. Therefore, the major spin states of V-3d are not filled, because although the doubly-degenerate state is completely filled, the triply-degenerate state is only one-third full. As a result, the three electrons produce a total magnetic moment of $2\mu_\beta$/atom-V. This implies that the magnetic moment has a value of μ=2 μ_β for one V atom present in the compounds $Al_{0.50}V_{0.50}N$ and $Al_{0.75}V_{0.25}N$, while μ=6 μ_β for three V atoms in $Al_{0.25}V_{0.75}N$ compound.

Figure 5 shows the band structures of the $Al_xV_{1-x}N$ (x=0.25, 0.50, and 0.75) ternary compounds. For x=0.25 and 0.50 ($Al_{0.25}V_{0.75}N$ and $Al_{0.50}V_{0.50}N$), Figures 5a and b confirm the half-metallic nature of both compounds, while Figure 5c confirms the metallic character of $Al_{0.75}V_{0.25}N$.

In Figure 5, it can seen that the spin-up orientation of the $Al_{0.25}V_{0.75}N$, $Al_{0.50}V_{0.50}N$ and $Al_{0.75}V_{0.25}N$ compounds exhibits dispersed bands above Fermi level; this confirm that the majority spin-up of V-3d is partially filled, and therefore, the fact that there is high polarization of the

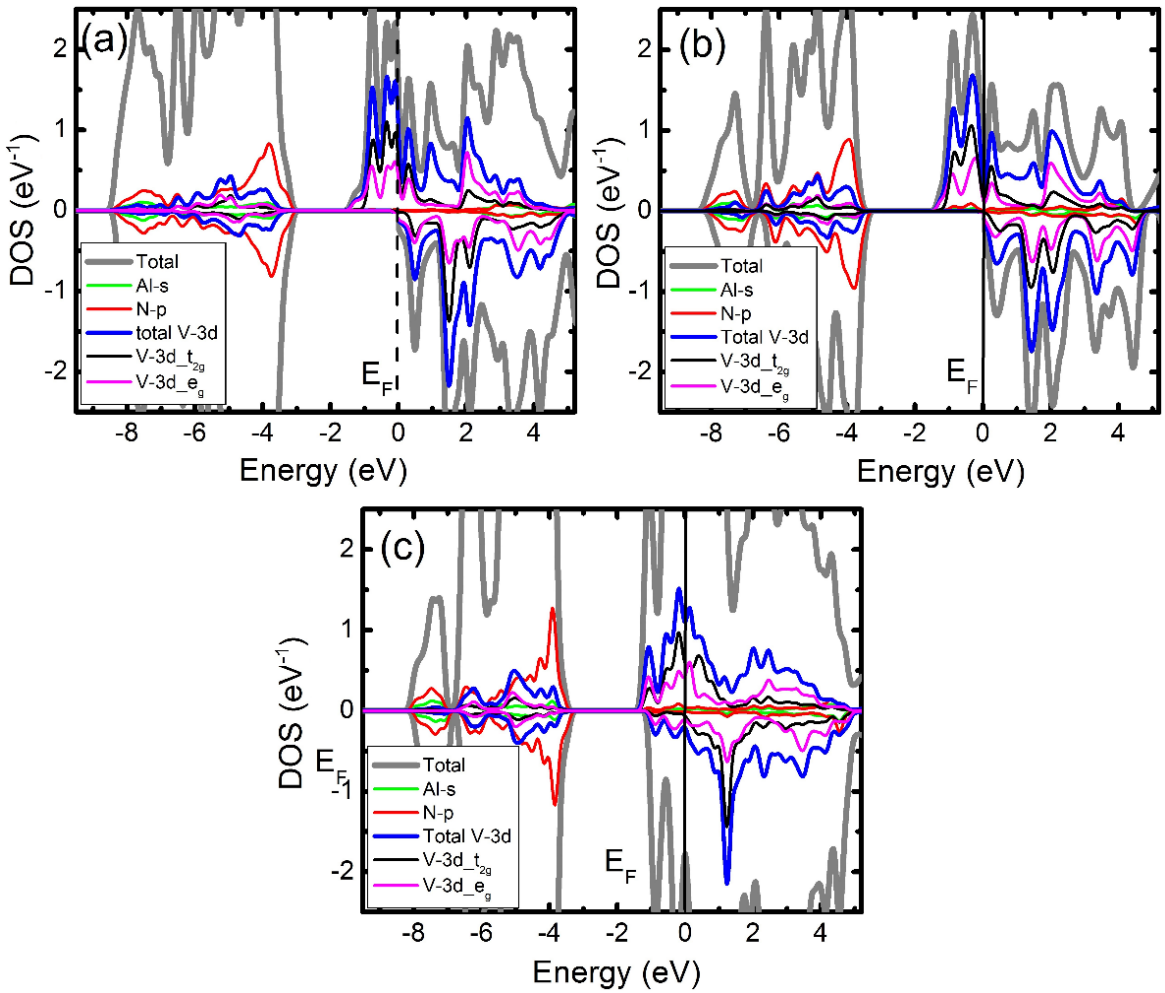

Figure 4. Total and partial density of states of the allowed ternary compounds of $Al_xV_{1-x}N$. (a) x = 0.25 (b) x = 0.50, and (c) x = 0.75.

conduction carriers is confirmed by the fact that the V atoms are coupling ferromagnetically and that there is a high presence of conduction carriers in the majority spin channel. For these reasons, these compounds can be potentially used in spintronics or spin injectors.

Conclusions

The authors report theoretical studies of the structural, electronic, and magnetic properties of $Al_xV_{1-x}N$ compounds, with concentrations of Al atoms x=0.0, 0.25, 0.50, 0.75, and 1.0, by means of first-principles calculations via the pseudopotential method, within the DFT framework and using the GGA approximation. It was found that the lattice constant increases with the concentration x of Al atoms, obeying a quadratic dependence. It was found that the values of the bulk modulus of $Al_xV_{1-x}N$ (x=0.25, 0.50, and 0.75) are high; therefore, these compounds are rigid and are good candidates for application in devices that must function at high temperatures and under high power, and in hard coatings. In addition, it was found that the allowed compounds $Al_{0.25}V_{0.75}N$ and $Al_{0.50}V_{0.50}N$ exhibit a half-metallic behavior with a magnetic moment of 2 μβ/atom-V. The ground-state ferromagnetic behavior essentially comes from the polarization of the V-3d that crosses the Fermi level. These compounds are good candidates for potential applications in spintronics and as spin injectors.

Conflict of Interest

The authors do not declare any conflict of interest.

ACKNOWLEDGEMENT

The authors thank the Research Center of the Distrital University Francisco José de Caldas CUID for its

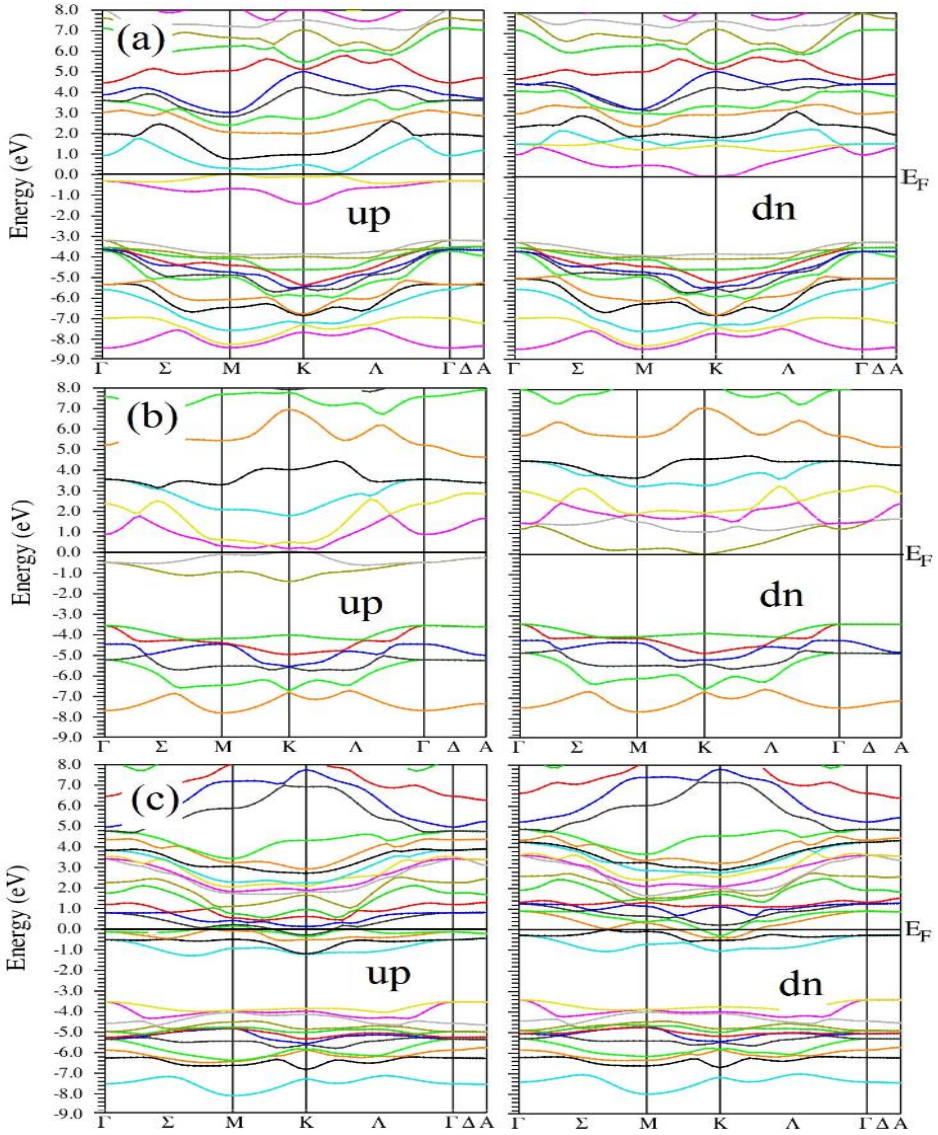

Figure 5. Band structure of allowed ternary compounds of $Al_xV_{1-x}N$. (a) x = 0.25 (b) x = 0.50, and (c) x = 0.75.

financial support.

REFERENCES

Beheshtian J, Baei MT, Bagheri Z, Peyghan AA (2012). AlN nanotube as a potential electronic sensor for nitrogen dioxide. Microelectron. J. 43(7):452-455. http://dx.doi:10.1016/j.mejo.2012.04.002

Boukra A, Zaoui A, Ferhat M (2010). Magnetic trends in $Ga_xMn_{1-x}N$, $Al_xMn_{1-x}N$, and $In_xMn_{1-x}N$ ternary systems: A first-principles study. J. Appl. Phys. 108:123904. http://dx.doi.org/10.1063/1.3524049

Carcia PF, French RH, Reilly ML, Lemon MF, Jones DJ (1997). Optical superlattices a strategy for designing phase-shift masks for photolithography at 248 and 193 nm: Application to AlN/CrN. Appl. Phys. Lett. 70:2371. http://dx.10.1063/1.118876

Carcia PF, French RH, Sharp K, Meth JS, Smith BW (1996). Materials screening for attenuating embedded phase-shift photoblanks for DUV and 193-nm photolithography. Proc. SPIE-Int. Soc. Opt. Eng. 2884:255-260. http://dx.doi.org/10.1117/12.262809

Dridi Z, Lazreg A, Bouhafs B (2011). First-principles study of electronic structure and magnetism of cubic $Al_{1-x}Er_xN$ using the LSDA+U approach. J. Magn. Magn. Mater. 323(9):1174-1178. http://dx.doi:10.1016/j.jmmm.2010.12.039

Frazier RM, Stepleton J, Thaler GT, Abernathy CR, Pearton SL, Rairigh R, Kelly J, Hebard AF, Nakarmi ML, Nam KB, Lin JY, Jiang HX, Zavada JM, Wilson RG (2003). Properties of Co-, Cr-, or Mn-implanted AlN. J. Appl. Phys. 94(3):1592. http://dx.10.1063/1.1586987

Giannozzi P, Baroni S, Bonin N (2009). QUANTUM ESPRESSO: a modular and open-source software project for quantum simulations of materials. J. Phys. Condens. Matter 21(39):395502. http:dx.doi:10.1088/0953-8984/21/39/395502

Gonzalez N, Majewski JA, Dietl T (2011). Aggregation and magnetism of Cr, Mn, and Fe cations in GaN. Phys. Rev. B 83:184417. http://dx.doi.org/10.1103/PhysRevB.83.184417

González R, López W, Rodríguez J (2007). AB initio studies of the structural and electronics properties of vanadium nitride. J. Ciencia

e Ingeniería Neogranadina 17(1):23-33. http://www.umng.edu.co/web/revistas/revistas-fac.ingenieria/revista-ciencia-e-ingenieria-neogranadina/revista-vol.-17-no.-1

Jonnard P, Capron N, Semond F, Massies J, Martinez-Guerrero E, Mariette H (2004). Electronic structure of wurtzite and zinc-blende AlN. Eur. Phys. J. B 42(3):351-359. http://dx.10.1140/epjb/e2004-00390-7

Katayama H, Sato K (2003). Spin and charge control method of ternary II-VI and III-Vmagnetic semiconductors for spintronics: theory vs. esperiment. J. Phys. Chem. Sol. 64:1447-1452-544. http://dx.10.1016/S0022-3697(03)00126-4

Laasonen K, Pasquarello A, Car R, Lee C, Vanderbilt D (1993). Car-Parrinello molecular dynamics with Vanderbilt ultrasoft pseudopotentials. Phys. Rev. B. 47:10142. http://dx.doi.org/10.1103/PhysRevB.47.10142

Lei WW, Liu D, Zhu PW, Chen XH, Zhao Q, Wen GH, Cui QL, Zou GT (2009). Ferromagnetic Sc-doped AlN sixfold-symmetrical hierarchical nanostructures. Appl. Phys. Lett. 95:162501. http://dx.doi.org/10.1063/1.3248257

Monkhorst HJ, Pack JD, (1976). Special points for Brillouin-zone integrations. Phys. Rev. B. 13(12):5188-5192. http://dx.doi.org/10.1103/PhysRevB.13.5188

Murnaghan FD (1944). The compressibility of media under pressure. Proceedings of the National Academy Science U.S.A. 30(9):244-247. http://www.ncbi.nlm.nih.gov/pmc/articles/PMC1078704/

Nakamura S, Senoh M, Nagahama S, Iwasa N, Yamada T, Matsushita T, Sugimoto Y, Kikoyu J (1997). High-Power, Long-Lifetime InGaN Multi-Quantum-Well-Structure Laser Diodes. Jpn. J. Appl. Phys. 36(8B):L1059. http://dx.doi:10.1143/JJAP.36.L1059

Perdew J, Burke K, Ernzerhof M (1997). Generalized Gradient Approximation Made Simple. Phys. Rev. Lett. 77(18):3865-3868. http://dx.doi.org/10.1103/PhysRevLett.77.3865

Schulz H, Thieman KH (1977). Crystal structure refinement of AlN and GaN. Solid State Communication 23(11):815-819. http://dx.10.1016/0038-1098(77)90959-0.

Sheng SH, Zhang RF, Veprek S (2008). Phase stabilities and thermal decomposition in the $Zr_{1-x}Al_xN$ system studied by ab initio calculation and thermodynamic modeling. Acta Materialia 56(5):968-976. http://dx.doi.org/10.1016/j.actamat.2007.10.050

Vanderbilt D (1990). Soft self-consistent pseudopotentials in a generalized eigenvalue formalism. Phys. Rev. B. 41:7892(R). http://dx.doi.org/10.1103/PhysRevB.41.7892

Vargas C, Espitia-Rico M, Báez Cruz R (2015). Half-metallic ferromagnetism of $Zn_xMn_{1-x}O$ compounds: A first-principles study. Comput. Condens. Matter 4:1-5. http://dx.doi:10.1016/j.cocom.2015.04.001

Warner JM, Bechstedt F (2002). Properties of strained wurtzite GaN and AlN: Ab initio studies. Phys. Rev. B 66:115202. http://dx.doi.org/10.1103/PhysRevB.66.115202

Wu QY, Huang ZQ, Wu R, Chen LJ (2007). Cu-doped AlN: a dilute magnetic semiconductor free of magnetic cations from first-principles study. J. Phys. Condens. Matter 19(5):056209. http://dx.doi:10.1088/0953-8984/19/5/056209

Wu RQ, Peng GW, Liu L, Feng YP, Huang ZG, Wu QY (2006). Ferromagnetism in Mg-doped AlN from ab initio study. Appl. Phys. Lett. 89:142501. http://dx.doi.org/10.1063/1.2358818

Wu SY, Liu HX, Gu L, Singh RK, Budd L, Schilfgaarde M, McCartney MR, Smith DJ, Newman N (2003). Synthesis, characterization and modeling of high quality ferromagnetic Cr-doped AlN thin films. Appl. Phys. Lett. 82:3047. http://dx.10.1063/1.1570521

Yang Y, Zhao Q, Zhang XZ, Liu ZG, Zou CX, Shen B, Yu DP (2007). Mn-doped AlN nanowires with room temperature ferromagnetic ordering. Appl. Phys. Lett. 90:092118. http://dx.doi.org/10.1063/1.2475276

Zhang RF, Veprek S (2007). Phase stabilities and spinodal decomposition in the $Cr_{1-x}Al_xN$ system studied by ab initio LDA and thermodynamic modeling: Comparison with the $Ti_{1-x}Al_xN$ and TiN/Si_3N_4 systems. Acta Mater. 55(14):4615-4619. http://dx.doi.org/10.1016/j.actamat.2007.04.029

Zhang Y, Liu W, Liang P, Niu HB (2008). Half-metallic ferromagnetism in Ca-doped AlN from first-principles study. Sol. State Commun. 147(7-8):254-257. Http://dx.doi:10.1016/j.ssc.2008.06.008


International Journal of Physical Sciences
Related Journals Published by Academic Journals
■African Journal of Pure and Applied Chemistry
■Journal of Internet and Information Systems
■Journal of Geology and Mining Research
■Journal of Oceanography and Marine Science
■Journal of Environmental Chemistry and Ecotoxicology
■Journal of Petroleum Technology and Alternative Fuels
academicJournals